Electronic Supplementary Information (ESI) for ChemComm.
This journal is © The Royal Society of Chemistry 2014

Electronic Supplementary Information For:

Aromatic Sulfonate Anion-Induced Pseudorotaxanes: Environmentally Benign Synthesis, Selectivity, and Structural Characterization

Han-Yuan Gong,*[a] Feng Tang,[b] Brett M. Rambo,[d] Rui Cao,*[b] Jun-Feng Xiang,*[c] Jonathan L. Sessler*[d]

[a]*College of Chemistry, Beijing Normal University, Beijing, 100875 (P. R. China);*

[b]*Department of Chemistry, Renmin University of China, Beijing, 100872 (P. R. China);*

[c]*Institute of Chemistry, Chinese Academy of Sciences, Beijing, 100190 (P. R. China);*

[d]*Department of Chemistry, Welch Hall 2.204, 105 E. 24TH ST. STOP A5300, The University of Texas at Austin, Austin, Texas, 78712-1224, USA*

Materials and Methods

Section S1: General considerations

All solvents were dried before use according to standard protocols.[1] For this study, all reagents were purchased commercially (Aldrich, Acros, or Fisher) and used without further purification. Deuterated solvents were purchased from Cambridge Isotope Laboratory (Andover, MA). NMR spectra were recorded on a Bruker Advanced instrument (500 MHz or 600 MHz for solution study). The ^{1}H and ^{13}C NMR chemical shifts are reported relative to residual solvent signals.[2]

The single crystals used to obtain the X-ray diffraction structures grew as colorless needles, plates, or prisms. The .cif documents are available from the Cambridge Crystallographic Data entre (CCDC) by quoting the appropriate file number given in Table S3 below. These files provide details regarding the specific crystals used for the analysis, along with the structure in question. Diffraction grade crystals were obtained by slow evaporation from solution using a mixture of water/actonitrile/N,N- dimethylformamide (DMF) or water/DMF as described below.

The data crystals were cut from the cluster of crystals and had the approximate dimensions given in the .cif documents. The data were collected on Rigaku Mercury2 (2x2 bin mode), Saturn724+ (2x2 bin mode) CCD, or Bruker APEX-II diffractometers using the graphite monochromator with MoKa radiation (λ = 0.71073 Å). The data were collected using w-scans with a scan range of 1° at low temperature using an Oxford Cryostream low temperature device. Data reduction was performed using DENZO-SMN.[3] The structures were solved by direct methods using SIR97[4] and refined by full-matrix least-squares on F^2 with anisotropic displacement parameters for the non-H atoms using SHELXL-97.[5] The hydrogen atoms were calculated in ideal positions with isotropic displacement parameters set to 1.2 x Ueq of the attached atom (1.5 x Ueq for methyl hydrogen atoms). The function $w(|Fo|^2 - |Fc|^2)^2$ was minimized. Definitions used for calculating R(F), Rw(F2) and the goodness of fit, S, are given

below and in the .cif documents.[6] Neutral atom scattering factors and values used to calculate the linear absorption coefficient are from the International Tables for X-ray Crystallography (1992).[7] All ellipsoid figures were generated using SHELXTL/PC.[8] Tables of positional and thermal parameters, bond lengths and angles, torsion angles, figures and lists of observed and calculated structure factors are located in the .cif documents available from the Cambridge Crystallographic Data Centre (CCDC) by quoting the CCDC no. 1012717-1012722 for each individual structure given in tables S3 below. The .cif documents also contain details of crystal data, data collection and structure refinement.

Section S2: Solution Binding studies and characterization of host-guest complexes in organic media

Studies of the host-guest binding interactions between $\mathbf{1}^{4+}\bullet 4PF_6^-$ and guest species 1,5-naphthalene disulfonate dianion (**2**), 2,6-naphthalene disulfonate dianion (**3**), and biphenyl-4,4′-disulfonate dianion (**4**) using ^{1}H-NMR spectroscopic methods. The addition of 2 molar equiv. of tetramethylammonium hydroxide ($TMA^+\bullet OH^-$) was found to be sufficient to fully deprotonated the aromatic disulfonic acid, and the subsequent binding interactions with macrocycle $\mathbf{1}^{4+}$ were investigated as detailed in the main text. Relevant plots are provided below.

Solution binding studies and characterization of the host-guest complex formed between 1^{4+} and 1,5-naphthalene disulfonate dianion (2):

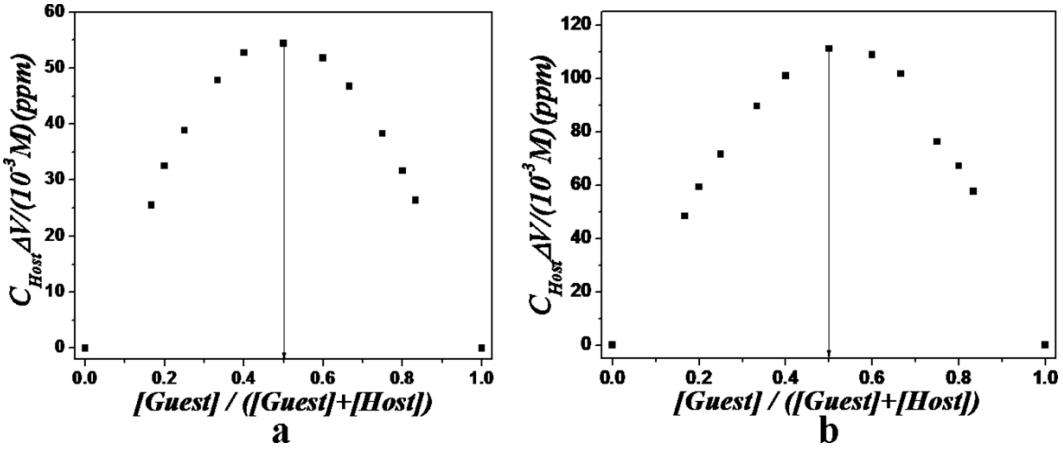

Figure S1. ^{1}H NMR spectroscopic Job-plots (600 MHz) corresponding to the binding between $\mathbf{1}^{4+}\bullet 4PF_6^-$ and **2** in [D_6]DMSO. (a) [host] + [guest] = 1×10^{-3} M and (b) [host] + [guest] = 2.5×10^{-3} M. At two concentrations the maximum value of y (defined as the product of chemical shift change value of H(1) on $\mathbf{1}^{4+}$ and the corresponding host concentration (i.e., [$\mathbf{1}^{4+}$]) was found when the mole fraction = 0.5, a finding consistent with a 1:1 (host: guest) binding stoichiometry.[9]

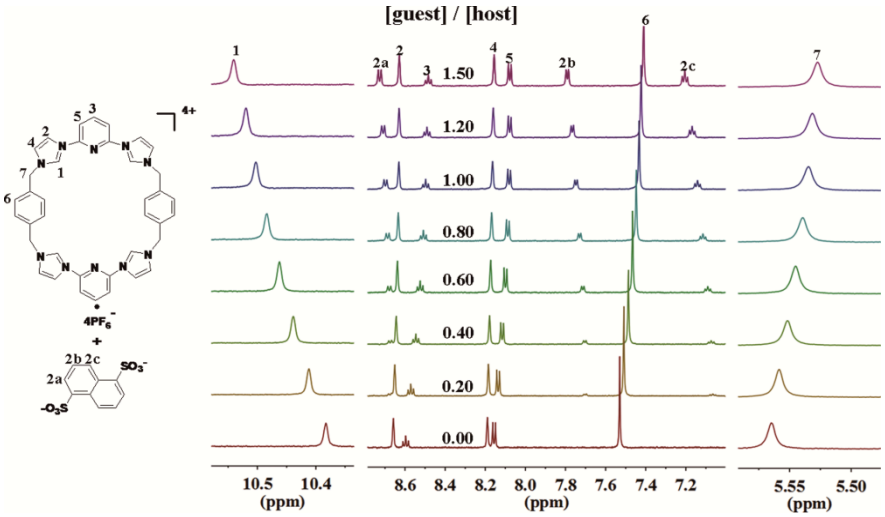

Figure S2. ^{1}H NMR spectroscopic titration of $\mathbf{1}^{4+}\bullet 4PF_6^-$ (5.00×10^{-4} M) with 1,5-naphthalene disulfonic acid in the presence of 2 molar equiv of $TMA^+\bullet OH^-$ (relative to **2**) in [D_6]DMSO at 300K (600 MHz).

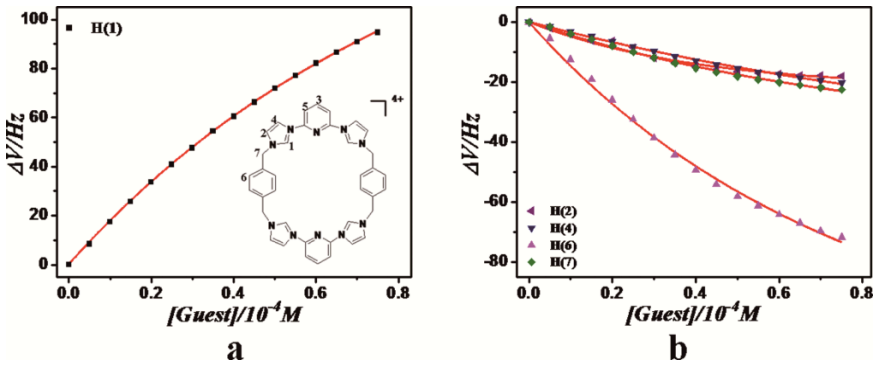

Figure S3. ^{1}H NMR binding isotherms corresponding to the interaction between $\mathbf{1}^{4+}\bullet 4PF_6^-$ and **2** in [D_6]DMSO at 300K. The chemical shift changes of (a) H(1), (b) H(2), H(4), H(6) and H(7) on $\mathbf{1}^{4+}$ were used for the calculation of K_1 ($(1.0 \pm 0.1) \times 10^3$ M^{-1}) using the Hyperquad 2003 program.[10] The chemical shift change of H(3) and H(5) were too small (less than 15.0 Hz) to be used in the calculation. The red dashed lines show the non-linear curve fit of the experimental data to the appropriate equation.

It was observed that the signals of H(2), H(3), H(4), H(5), H(6) and H(7) on $\mathbf{1}^{4+}$ were shifted to higher fields upon the addition of anion **2**. These changes provide initial evidence that π-π donor-acceptor interactions are involved in the formation of a complex with a 1:1 host:guest stoichiometry (*cf.* Figure S3b). The observed binding interactions were postulated to result from

the different planar fragments present in $\mathbf{1}^{4+}$, namely the 1,4-bis-methylbenzene and 2,6-di(1H-imidazol-1-yl)pyridine subunits, acting as π-electron acceptors capable of anion binding. Separately, 2D-DOSY spectroscopic analyses provided evidence that a stable complex was formed between host $\mathbf{1}^{4+}$ and guest **2**. All of the protons, including those located on $\mathbf{1}^{4+}$ and **2**, showed similar diffusion times in the representative solution state mixtures (*cf.* Figure S4).

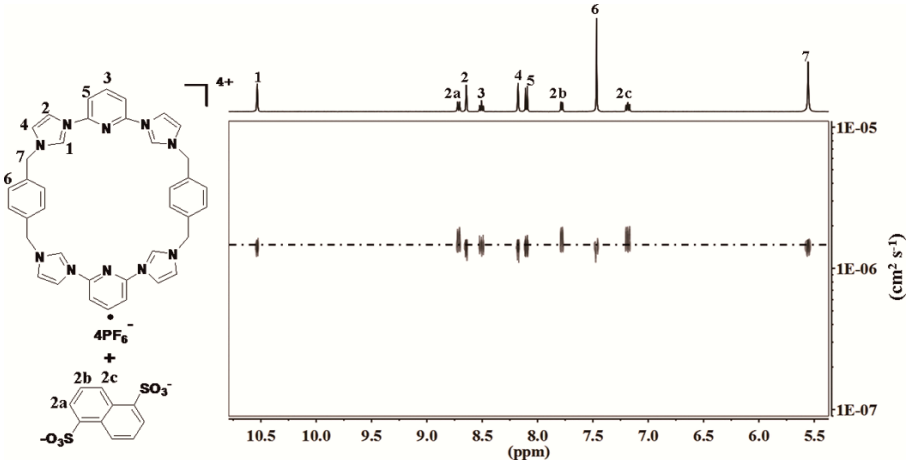

Figure S4. Expanded view of the 600 MHz 2D-DOSY NMR spectrum of $\mathbf{1}^{4+}$•$4PF_6^-$ (2.50 mM) recorded in the presence of 1 molar equiv. of **2** and 2 molar equiv. of TMA^+•OH^- in $[D_6]$DMSO at 300K.

The NOESY spectroscopic study was carried out in an effort to elucidate the nature of the host-guest interactions between $\mathbf{1}^{4+}$ and guest **2** that are operative in solution. No correlation between host and guest was observed in this study. The spectrum was consistent with coordination through the "outside" binding mode shown in Scheme 1 of the main text (*cf.* Figure S5).[11-13]

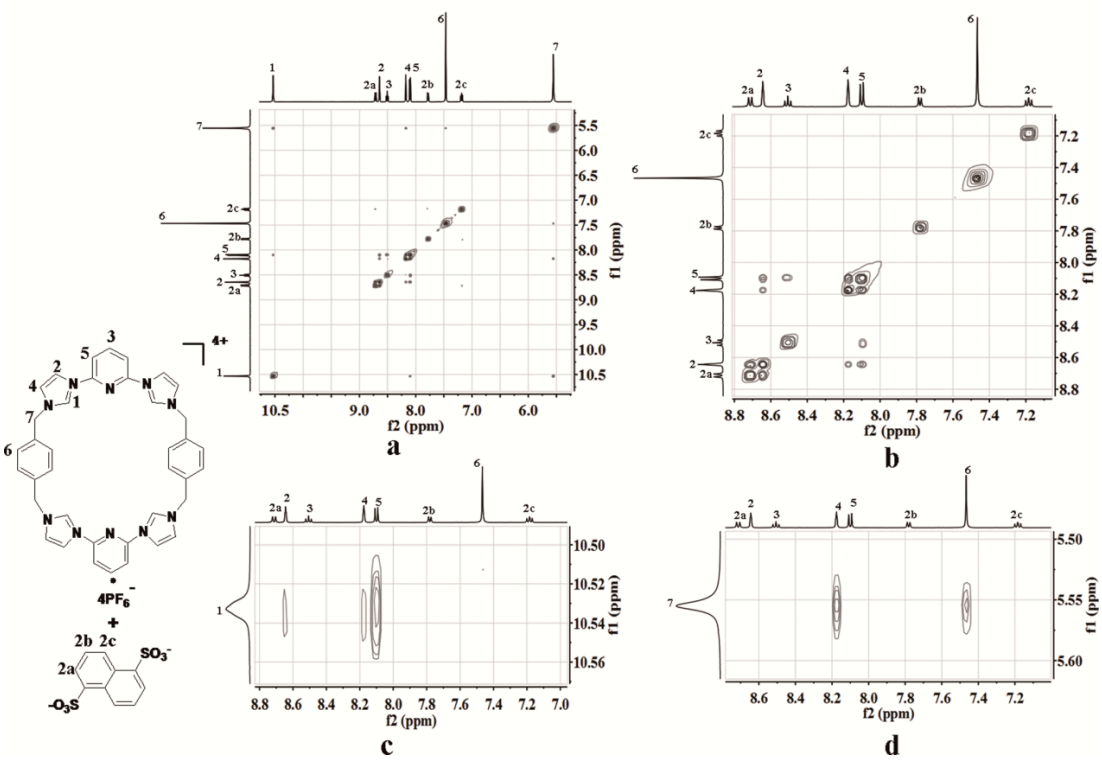

Figure S5. Full view (a) and expanded view (b, c and d) of the 600 MHz NOESY NMR spectra of $\mathbf{1}^{4+}$•$4PF_6^-$ (2.50 mM) recorded in the presence of 1 molar equiv. of **2** and 2 molar equiv. of TMA^+•OH^- in [D_6]DMSO at 300K.

Solution binding studies and characterization of the host-guest complex formed from 1^{4+} and the 2,6-naphthalene disulfonate dianion (3):

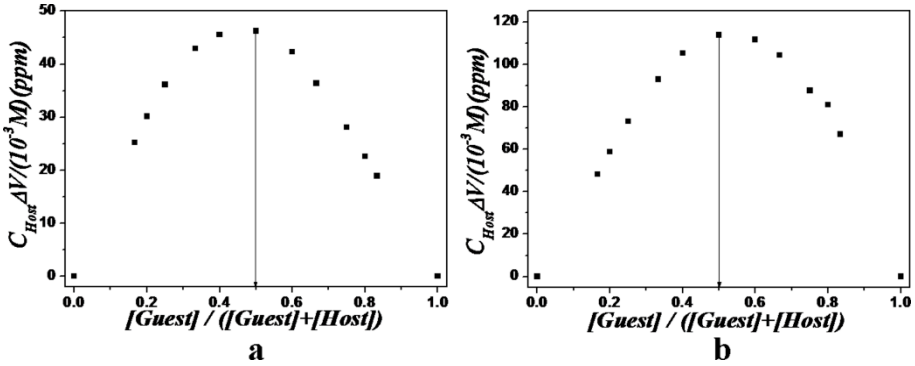

Figure S6. ^{1}H NMR Job-plots (600 MHz) corresponding to the binding between $\mathbf{1}^{4+}$•$4PF_6^-$ and **3** in [D_6]DMSO ((a) [host] + [guest] = 1×10^{-3} M and (b) [host] + [guest] = 2.5×10^{-3} M). At the two test concentrations used herein, the maximum value of y (defined as the product of chemical shift change value of H(1) on $\mathbf{1}^{4+}$ and the corresponding host concentration (i.e., [$\mathbf{1}^{4+}$]), was found at 0.5. This finding is consistent with a 1:1 (host: guest) binding stoichiometry.[9]

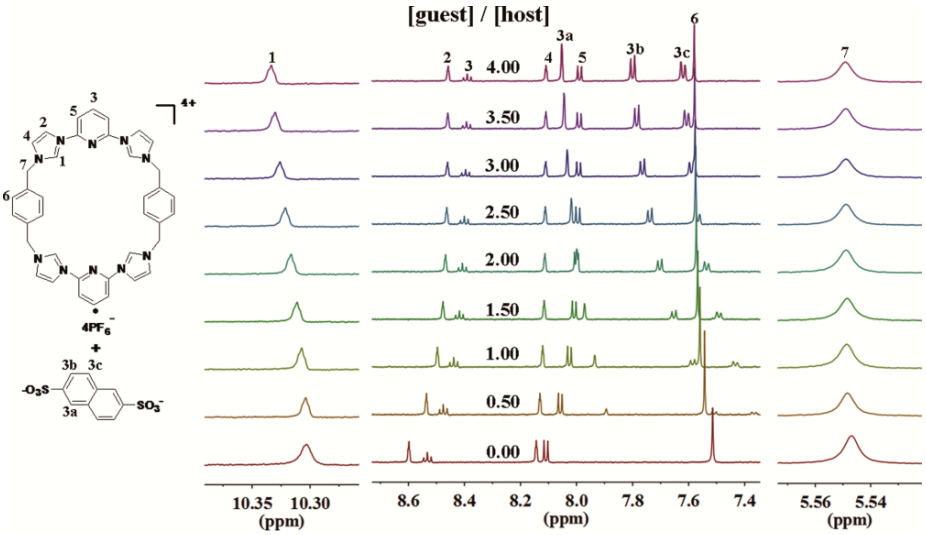

Figure S7. ^{1}H NMR spectroscopic titration of $\mathbf{1}^{4+}\bullet 4PF_6^-$ (5.00×10^{-4} M) with **3** in the presence of 2 molar equiv. of $TMA^+\bullet OH^-$ (relative to **3**) in [D_6]DMSO at 300K (600 MHz).

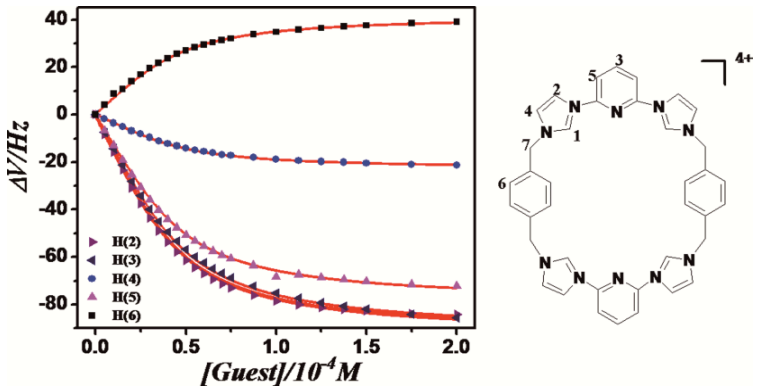

Figure S8. ^{1}H NMR binding isotherms corresponding to the interaction between $\mathbf{1}^{4+}\bullet 4PF_6^-$ and **3** in [D_6]DMSO at 300K. The chemical shift changes of H(2) and H(3), H(4), H(5) and H(6) on $\mathbf{1}^{4+}$ were used for the calculation of K_1 ($(1.6 \pm 0.1) \times 10^4$ M^{-1}) using the Hyperquad 2003 program.[10] The chemical shift change of H(1) and H(7) were too small (less than 20.0 Hz) to be used in the calculation. The red dashed lines show the non-linear curve fit of the experimental data to the appropriate 1:1 binding equation.

It was observed that the signals of H(2), H(3), H(4) and H(5) were shifted to higher fields upon the addition of **3**. These changes provide evidence that π-π donor-acceptor interactions between the aromatic ring of the anion and the 2,6-di(1H-imidazol-1-yl) pyridine fragments on $\mathbf{1}^{4+}$ are involved in complex formation (1:1 stoichiometry (host: guest)). Very different binding interactions were observed between **3** and the bridged 1,4-bis-methylbenzene present in $\mathbf{1}^{4+}$, as

compared with the interactions observed between $\mathbf{1}^{4+}$ and **2**. The addition of 1.5 molar equiv. of guest **2** caused H(6) on $\mathbf{1}^{4+}$ to shift to higher field (71.8 Hz), while the same amount of **3** caused H(6) on $\mathbf{1}^{4+}$ to shift to lower field (32.1 Hz). Further, the peak ascribed to H(1) displayed a less pronounced shift to lower field upon the addition of guest **3** (Δδ 4.7 Hz), as compared to that observed upon the addition of guest **2** (Δδ 94.7 Hz). In both cases, 1.5 molar equiv. of the anion were used. The shifts of H(1), which are the strongest acidic protons present on $\mathbf{1}^{4+}$, are considered key indicators of intermolecular hydrogen bonds between the host macrocycle and the anionic guest. Thus, we propose that the larger chemical shift change of H(1) observed upon the addition of guest **3** is consistent with the presence of stronger π-π donor-acceptor interactions between $\mathbf{1}^{4+}$ and **3**, as compared to occurs when $\mathbf{1}^{4+}$ is mixed with **2** under identical conditions (*cf.* Figure S8).

2D-DOSY spectroscopic analysis provided further evidence that a stable complex was constructed between the host $\mathbf{1}^{4+}$ and guest anion **3**. All the protons, including those on $\mathbf{1}^{4+}$ and **3**, showed similar diffusion times when analyzed as solution state mixtures (*cf.* Figure S9).

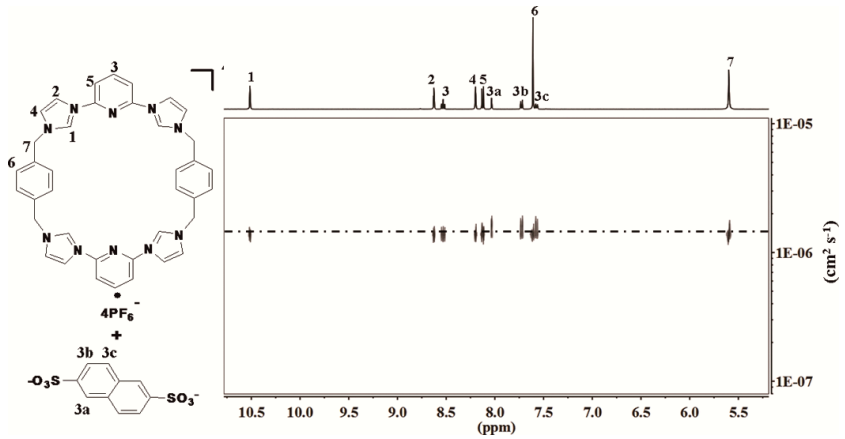

Figure S9. Expanded view of the 600 MHz 2D-DOSY NMR spectrum of $\mathbf{1}^{4+}\bullet 4PF_6^-$ (2.50 mM) recorded in the presence of 1 molar equiv. of 2,6-naphthalene disulfonic acid **3** and 2 molar equiv of $TMA^+\bullet OH^-$ (relative to **3**) in [D_6]DMSO at 300K.

NOESY NMR spectroscopic studies were carried out in an effort to elucidate the nature of the host-guest interactions between macrocycle $\mathbf{1}^{4+}$ and **3** in [D_6]DMSO solution. In the resulting spectra, correlations between H(1) and H(3b, 3c), H(5) and H(3a), H(6) and H(3b), H(7) and H(3a, 3b) were observed. The spectra, shown in Figure S10, are consistent with the threaded binding mode shown in Scheme 1 of the main text.[11-13]

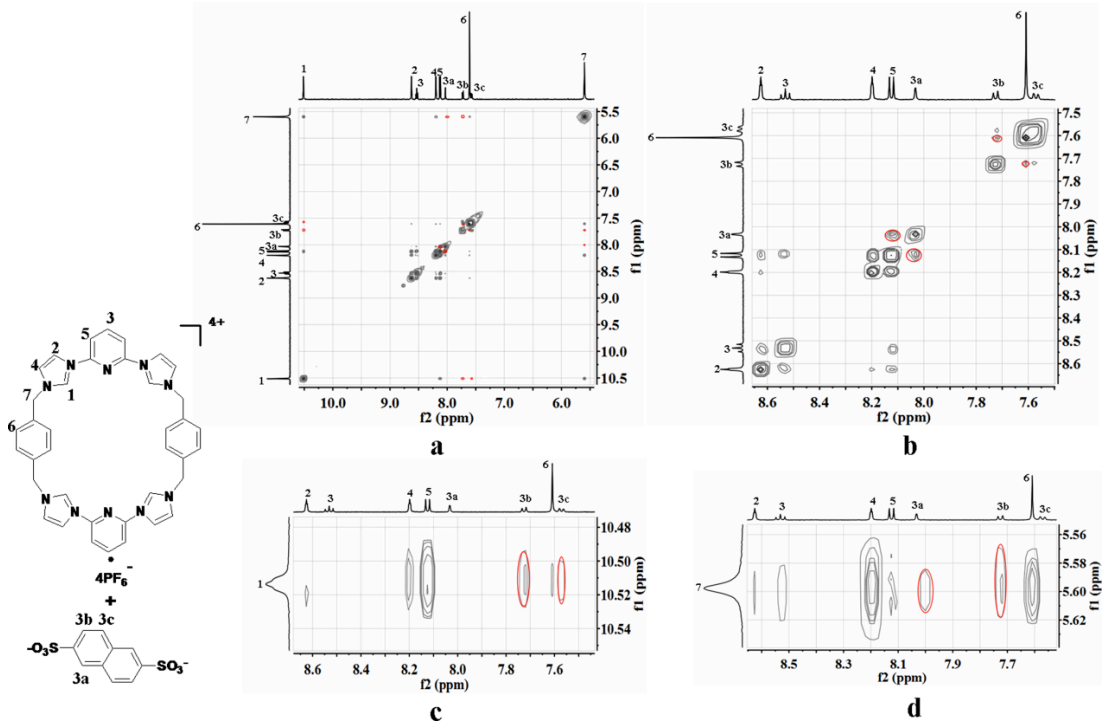

Figure S10. Full view (a) and expanded view (b, c and d) of the 600 MHz NOESY NMR spectra of $\mathbf{1}^{4+}$•4PF_6^- (2.50 mM) recorded in the presence of 1 molar equiv. of 2,6-naphthalene disulfonic acid **3** and 2 molar equiv. of TMA^+•OH^- (relative to **3**) in [D_6]DMSO at 300K.

Solution binding studies and characterization of the host-guest complex formed between 1^{4+} and the biphenyl-4,4′-disulfonate dianion (4):

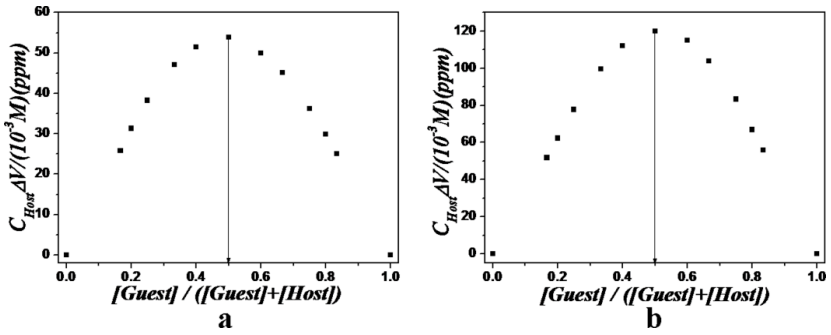

Figure S11. 600 MHz ^{1}H NMR Job-plots corresponding to the binding between $\mathbf{1}^{4+}$•4PF_6^- and **4**. (a) [host] + [guest] = 1 × 10^{-3} M and (b) [host] + [guest] = 2.5 × 10^{-3} M. At the two concentrations used, the maximum value of y (defined as the product of chemical shift change value of H(1) on $\mathbf{1}^{4+}$ and the corresponding host concentration (i.e., [$\mathbf{1}^{4+}$]), was found at 0.5. This finding is consistent with a 1:1 (host: guest) binding stoichiometry.[9]

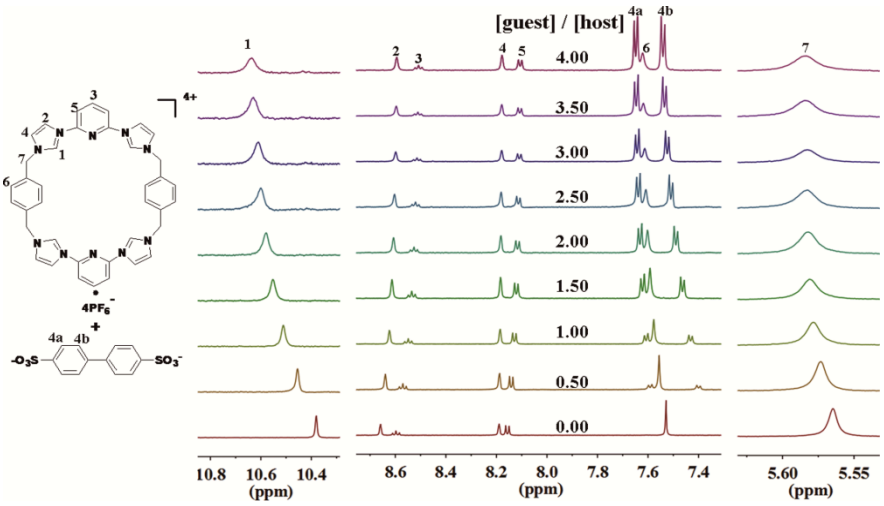

Figure S12. 600 MHz ^{1}H NMR spectroscopic titration of $\mathbf{1}^{4+}$•4PF_6^- (5.00×10^{-4} M) with **4** in the presence of 2 molar equiv. of TMA^+•OH^- (relative to **4**) in [D_6]DMSO at 300K.

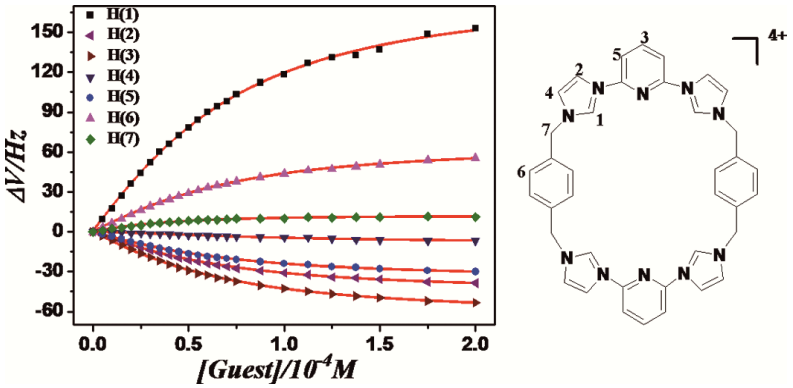

Figure S13. ^{1}H NMR binding isotherms corresponding to the interaction between $\mathbf{1}^{4+}$•4PF_6^- and **4** in [D_6]DMSO at 300K. The chemical shift changes of all the protons on $\mathbf{1}^{4+}$ were used for the

calculation of K_1 ((3.0 ± 0.2) × 10^3 M^{-1}) using the Hyperquad 2003 program.[10] The red dashed lines show the non-linear curve fit of the experimental data to the appropriate 1:1 binding equation.

It was observed that the signals of H(2), H(3), H(4) and H(5) were shifted to higher field upon the addition of the biphenyl-4,4′-disulfonate dianion (**4**). These changes provide initial evidence that π-π donor-acceptor interactions between the aromatic ring of the anion and the 2,6-di(1H-imidazol-1-yl)pyridine fragments on $\mathbf{1}^{4+}$ are involved in the formation of a 1:1 complex (stoichiometry inferred from the Job plot; vide supra). In this case, similar interactions were observed between **4** and the bridged 1,4-bis-methylbenzene present in $\mathbf{1}^{4+}$ as seen in the case or receptor $\mathbf{1}^{4+}$ and guest **3**. However, in the case of **4**, the peak ascribed to H(1) undergoes the largest shift to lower field (Δδ = 103.1 Hz) upon the addition of 1.5 molar equiv. of guest **4**. These findings provide support for the conclusion that intermolecular hydrogen bonding and π-π donor-acceptor interactions co-stabilize the complex formed between receptor $\mathbf{1}^{4+}$ and guest **4** (*cf.* Figure S13).

A 2D-DOSY spectroscopic analysis revealed that all the protons, including those on $\mathbf{1}^{4+}$ and **4**, were characterized by similar diffusion times when mixed in [D_6]DMSO at 300K (*cf.* Figure S14). As noted in the main text, this is taken as evidence that a stable complex is formed between host $\mathbf{1}^{4+}$ and the anionic guest **4**.

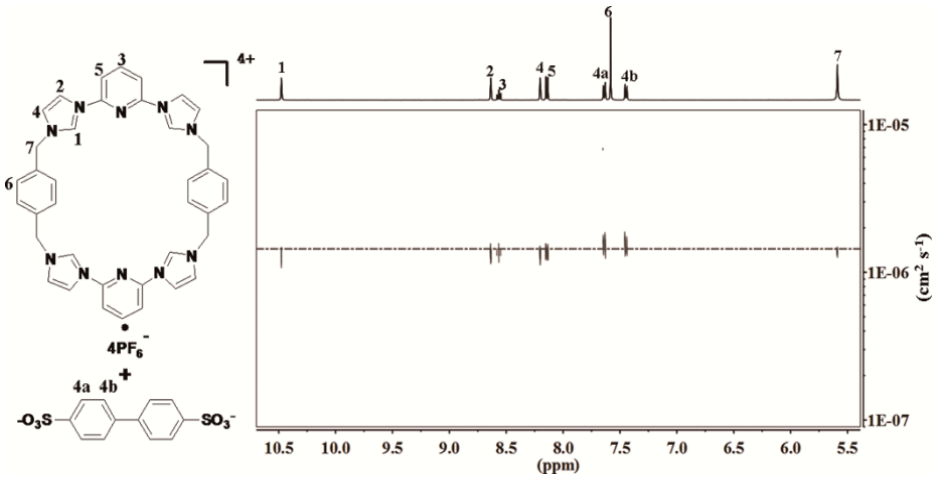

Figure S14. Expanded view of the 600 MHz 2D-DOSY NMR spectrum of $\mathbf{1}^{4+}\bullet 4PF_6^-$ (2.50 mM) recorded in the presence of 1 molar equiv. of **4** and 2 molar equiv. of $TMA^+\bullet OH^-$ in $[D_6]$DMSO at 300K.

NOESY NMR spectroscopic studies were carried out in an effort to elucidate the nature of the host-guest interactions between macrocycle $\mathbf{1}^{4+}$ and **4** that are pertinent in $[D_6]$DMSO solution. Correlations between H(1) and H(4b), H(2) and H(4a, 4b), H(3) and H(4a), H(4) and H(4a, 4b), H(5) and H(4a,4b), H(6) and H(4b), H(7) and H(4b) were observed. The spectra are consistent with the threaded binding mode shown in Scheme 1 of the main text (*cf.* also Figure S15).[11-13]

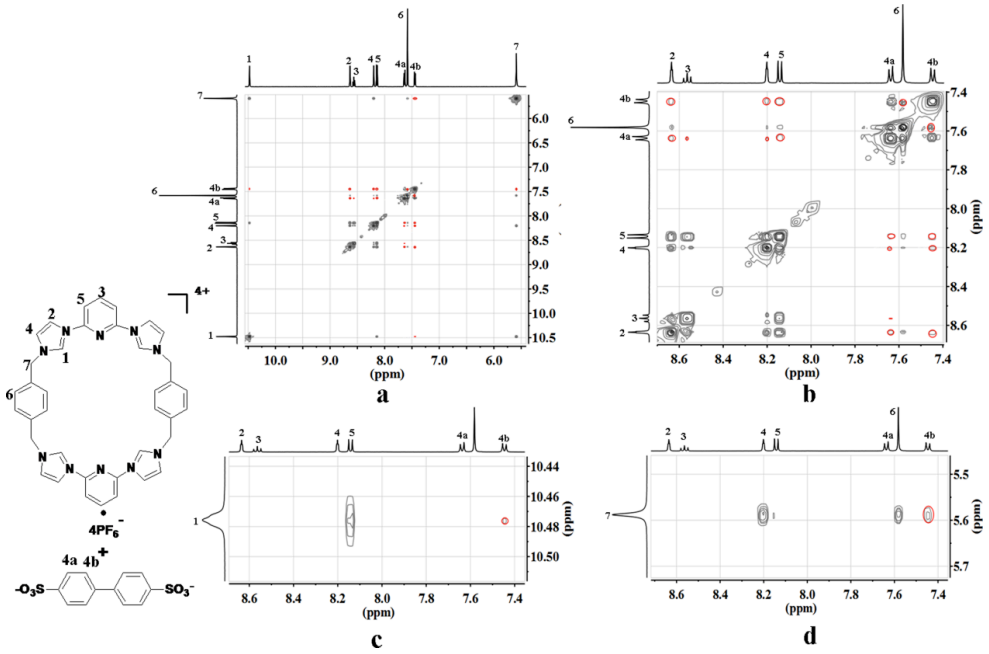

Figure S15. Full and expanded views of the 600 MHz NOESY NMR spectra of $\mathbf{1}^{4+}\bullet 4PF_6^-$ (2.50

mM) recorded in the presence of 1 molar equiv. of the biphenyl-4,4′-disulfonic acid **4** and 2 molar equiv. of TMA^{+}•OH^{-} in [D_6]DMSO at 300K.

An additional UV-vis spectroscopic study was carried out. Compared with $\mathbf{1}^{4+}$, the absorbance of complex $[\mathbf{1}^{4+}\bullet\mathbf{n}]^{2+}$ (**n** = **2**, **3**, or **4**) was characterized by a small red shift. However, there is no charge-charge transfer band apparent in the long wavelength spectral region.

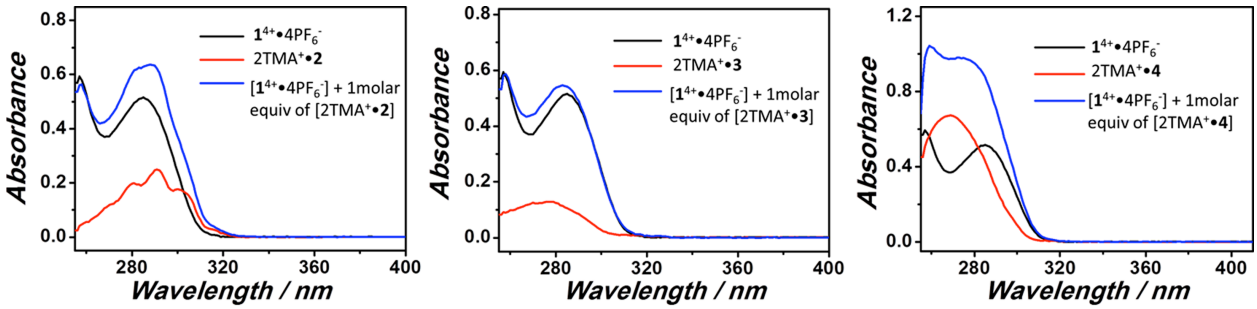

Figure S16. UV-vis spectra of $\mathbf{1}^{4+}\cdot 4PF_6^{-}$ (6.00×10^{-5} M), $2TMA^{+}\cdot\mathbf{n}$ (6.00×10^{-5} mM), and $\mathbf{1}^{4+}\cdot 4PF_6^{-}$ (6.00×10^{-5} mM) in the presence of 1 molar equiv. of **2** (a), **3** (b), or **4** (c) recorded using a 0.5 cm optical length in DMSO.

Section S3: Mass spectrometric studies

Electrospray mass spectrometry (ESI-MS) analyses of $\mathbf{1}^{4+}$ carried in the presence of each of the guest moieties **2**, **3** and **4** produced several ions consistent with the formation of gas phase host/guest complexes (*i.e.* Table S1).

Table S1. Summary of ESI-MS results are shown below. Peak assignments were confirmed by collisional activation (fragmentation) experiments, which produced ions corresponding to the free host $\mathbf{1}^{4+}$ in all cases.

Summary of ESI results (*m/z*)

Compound	Observed Peak	Proposed m/z Assignment
$\mathbf{1}^{4+}\bullet\mathbf{2}_2$	458.1 622.7 915.2 951.2 1203.2	$[\mathbf{1}^{4+} + \mathbf{2}\ ]^{2+}$ $[\mathbf{1}^{4+} + \mathbf{2} + 2Na - 3H]^{2+\bullet}$ $[\mathbf{1}^{4+} + \mathbf{2} - H]^{+\bullet}$ $[\mathbf{1}^{4+} + \mathbf{2} + K - 4H]^{+\bullet}$ $[\mathbf{1}^{4+} + \mathbf{2}_2 + K - 4H]^{+\bullet}$
$\mathbf{1}^{4+}\bullet\mathbf{3}_2$	458.1 610.8 915.2 961.3	$[\mathbf{1}^{4+} + \mathbf{3}\ ]^{2+}$ $[\mathbf{1}^{4+} + \mathbf{3}_2 + Na - 4H]^{+\bullet}$ $[\mathbf{1}^{4+} + \mathbf{3} - H]^{+\bullet}$ $[\mathbf{1}^{4+} + \mathbf{3} + 2Na - H]^{+\bullet}$
$\mathbf{1}^{4+}\bullet\mathbf{4}_2$	471.1 549.1 687.8 785.1	$[\mathbf{1}^{4+} + \mathbf{4}]^{2+}$ $[(\mathbf{1}^{4+})_2 + \mathbf{4} - 3H]^{3+\bullet}$ $[\mathbf{1}^{4+} + \mathbf{4}_2 + 2K + 2Na - 2H]^{2+\bullet}$ $[(\mathbf{1}^{4+})_2 + \mathbf{4} - 2H]^{2+\bullet}$

Section S4: Solution state binding studies and characterization of host-guest complexes in aqueous media

Synthesis of cyclo[2](2,6-di(1H-imidazol-1-yl)pyridine)[2](1,4-dimethylenebenzene) tetra -chlorate [1^{4+}•4Cl⁻]:

A solution of cyclo[2](2,6-di(1H-imidazol-1-yl)pyridine)[2](1,4-dimethylenebenzene) hexafluorophosphate [$\mathbf{1}^{4+}$•4PF_6^-] (500.0 mg, 13.8 mmol) in acetonitrile (30 ml) was added dropwise to a solution of tetrabutylammonium chloride (1148 mg, 206.5 mmol) in acetonitrile (20 ml) while stirring. The solution was stirred for half an hour after which point a white precipitate was collected and washed with 50 mL acetonitrile. The solid material was then dried at 393K for 1.5 hours. This gave rise to the colorless tetrakis chloride anion salt in quantitative yield (yield in 99.5%, 317.6 mg). m.p.: 302-304 ºC (decomp.); ^{1}H NMR (600 MHz, D_2O, 298K) δ 8.44 (t, 2H, *J* = 8.2 Hz, H_γ-Py), 8.30 (m, 4H, imidazolium ring -CH=C**H**-N-Py), 8.02 (d, 4H, *J* = 8.2 Hz, H_β-Py), 7.83 (m, 4H, imidazolium ring -CH=C**H**-N-CH_2-), 7.53 (s, 8H, Ar*H*), 5.63 (s, 8H, -C-C**H**$_2$-N-); ^{13}C NMR (150 MHz, D_2O, 298K) *δ* 146.8, 146.2, 135.7, 130.4, 125.4, 121.2, 116.4, 54.4; FT-ICRMS: calcd. for [$\mathbf{1}^{4+}$ + 2Cl^-]$^{2+}$ 350.1173; Found: 350.1167.

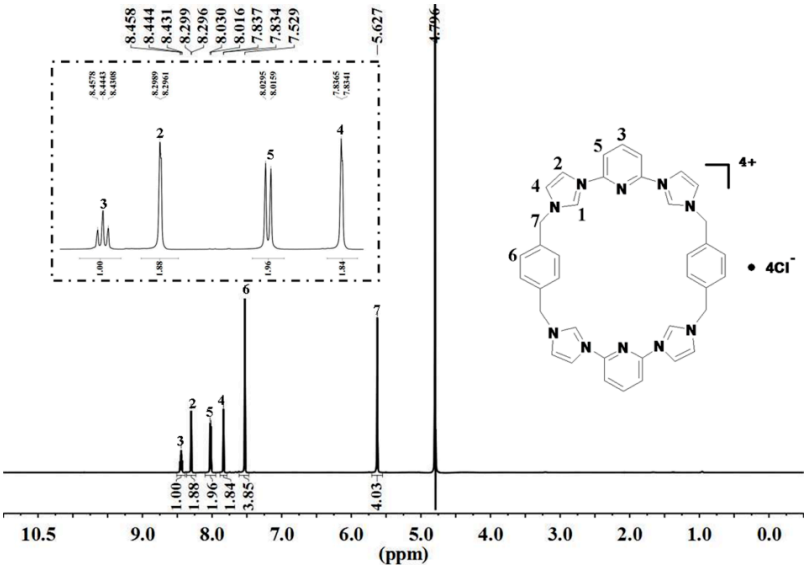

Figure S17. ^{1}H NMR spectrum of [$\mathbf{1}^{4+}$•4Cl^-] in D_2O at 298K.

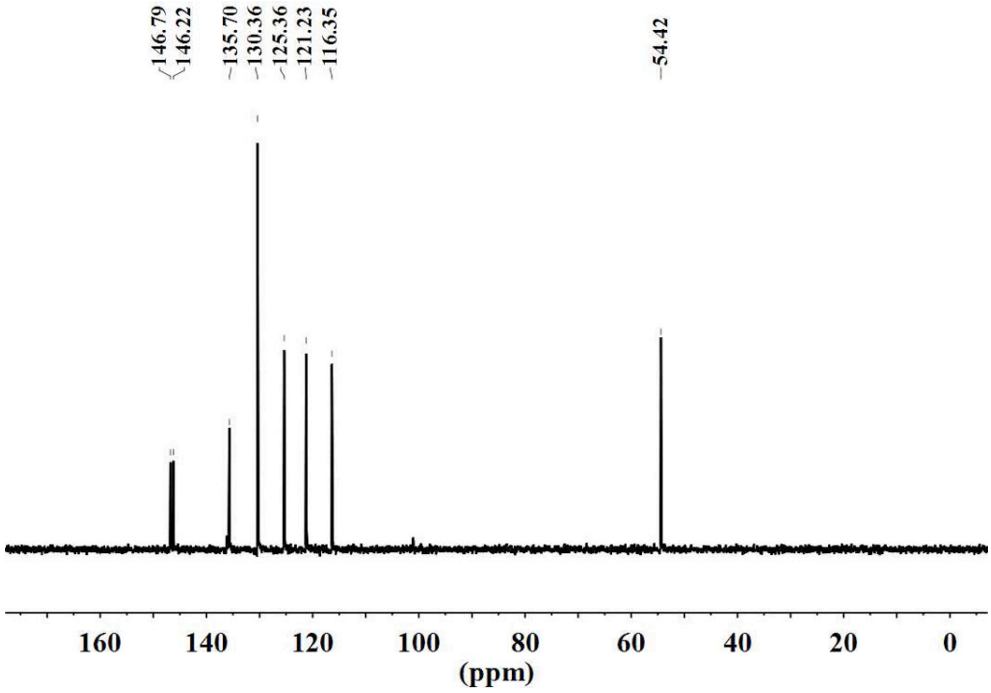

Figure S18. ^{13}C NMR spectrum of [$\mathbf{1}^{4+}$•4Cl$^-$] in D_2O at 298K.

Solution binding studies and characterization of host-guest complex formed from 1^{4+} and the 1,5-naphthalene disulfonate dianion (2) in D_2O:

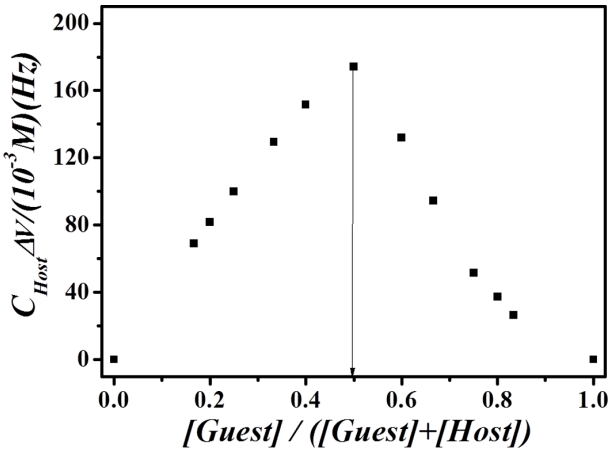

Figure S19. ^{1}H NMR Job-plots (600 MHz) corresponding to the binding between $\mathbf{1}^{4+}$•4Cl$^-$ and **2** in D_2O ([host] + [guest] = 1×10^{-3} M) in D_2O. The maximum value of y (defined as the product of chemical shift change value of H(3) on $\mathbf{1}^{4+}$ and the corresponding host concentration (i.e., [$\mathbf{1}^{4+}$]) was found at 0.5, a finding consistent with a 1:1 (host: guest) binding stoichiometry.[9]

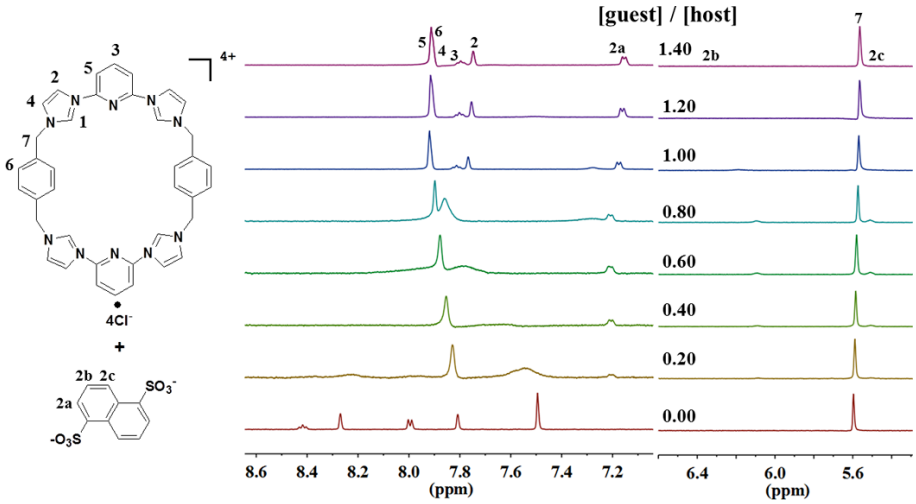

Figure S20. ^{1}H NMR spectroscopic titration of $\mathbf{1}^{4+}$•4Cl^{-} (5.00×10^{-4} M) with **2** in the presence of 2 molar equiv of NaOH (relative to **2**) in D_2O at 300K (600 MHz).

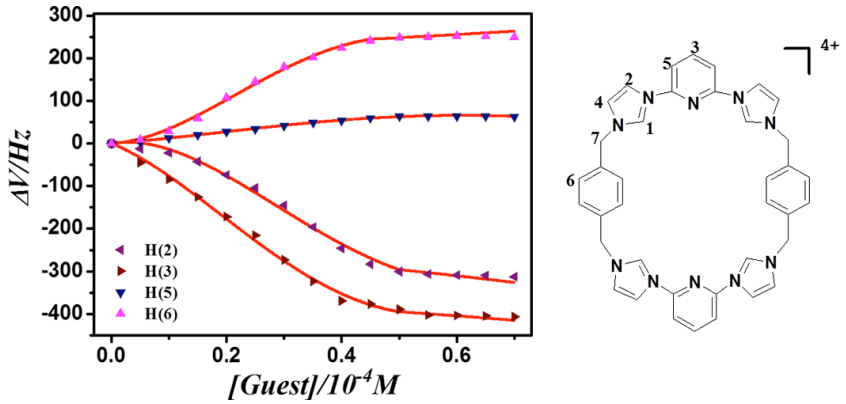

Figure S21. ^{1}H NMR binding isotherms corresponding to the interaction between $\mathbf{1}^{4+}$•4Cl^{-} and **2** in D_2O at 300K. The Gaussian function peak split technique was used for peak chemical shift confirmation.[11] The chemical shift changes of H(2), H(3), H(5) and H(6) on $\mathbf{1}^{4+}$ were used for the calculation of K_1 ($(3.5 \pm 0.2) \times 10^{3}$ M^{-1}) using the Hyperquad 2003 program.[10] The chemical shift changes of H(4) and H(7) were too small (less than 12.0 Hz) to be used in the calculation. The red dashed lines show the non-linear curve fit of the experimental data to the appropriate 1:1 binding equation.

It was observed that the signals of H(2), H(3) and H(5) were shifted to higher field upon the addition of **2**. These changes were taken as evidence that interactions between the aromatic ring of the anion and the 2,6-di(1H-imidazol-1-yl) pyridine fragments on $\mathbf{1}^{4+}$ are involved in complex formation (stoichiometry inferred as 1:1 (host: guest) based on Job plots; *vide supra*).

A 1D NOESY spectroscopic study between macrocycle $\mathbf{1}^{4+}$ and **2** was also carried out. There is no clear evidence that an interpenetrated structure is formed (*cf.* Figure S22).

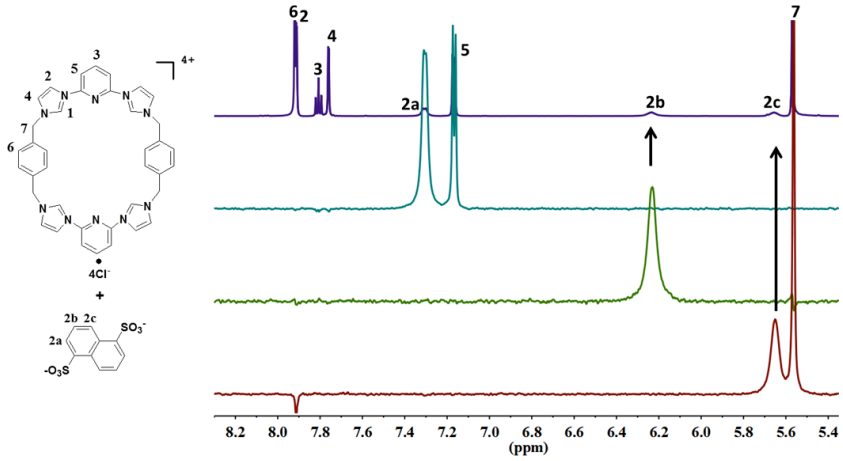

Figure S22. Expansion of the 1D ^{1}H NMR spectrum (top) and the corresponding selective 1D NOE NMR spectrum. The spectrum was obtained through irradiation at the frequencies corresponding to H(2a, 2b, or 2c) (from top to bottom) of **2** in the presence of 1 molar equiv (relative to **2**) of $\mathbf{1}^{4+}\cdot 4Cl^-$ (2.50 mM). The study was carried out in D_2O at 300 K (600 MHz).

Solution binding studies and characterization of host-guest complex formed from 1^{4+} and the 2,6-naphthalene disulfonate dianion (3) in D_2O:

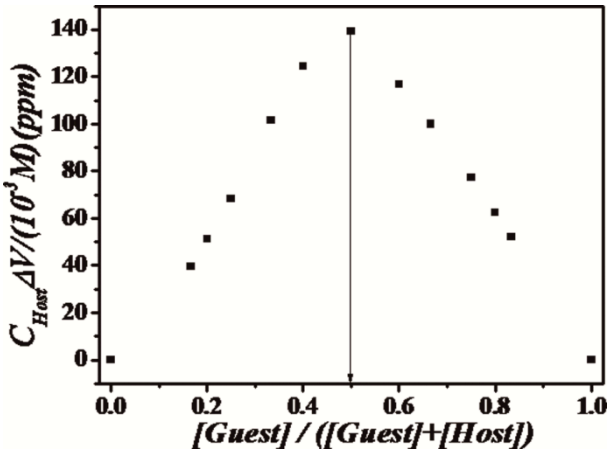

Figure S23. ^{1}H NMR Job-plots (600 MHz) corresponding to the binding between $\mathbf{1}^{4+}\bullet 4Cl^-$ and **3** in D_2O ([host] + [guest] = 1×10^{-3} M) in D_2O. The maximum value of y (defined as the product of chemical shift change value of H(3) on $\mathbf{1}^{4+}$ and the corresponding host concentration (i.e., [$\mathbf{1}^{4+}$]) was found at 0.5, a finding consistent with a 1:1 (host: guest) binding stoichiometry.[9]

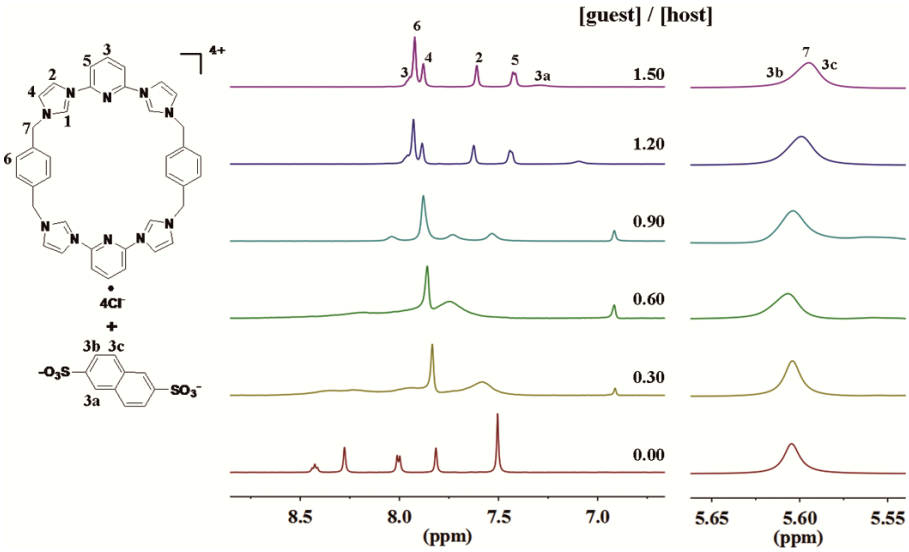

Figure S24. ^{1}H NMR spectroscopic titration of $\mathbf{1}^{4+}$•4Cl^{-} (5.00×10^{-4} M) with **3** in the presence of 2 molar equiv of NaOH (relative to **3**) in D_2O at 300K (600 MHz).

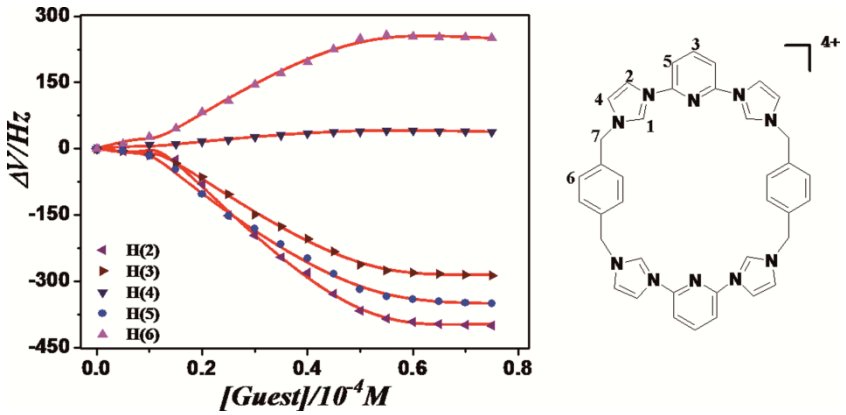

Figure S25. ^{1}H NMR binding isotherms corresponding to the interaction between $\mathbf{1}^{4+}$•4Cl^{-} and **3** in D_2O at 300K. The Gaussian function peak split technique was used for peak chemical shift confirmation.[11] The chemical shift changes of H(2), H(3), H(4), H(5) and H(6) on $\mathbf{1}^{4+}$ were used for the calculation of K_1 ($(3.4 \pm 0.2) \times 10^5$ M^{-1}) using the Hyperquad 2003 program.[10] The chemical shift change of H(7) were too small (less than 6.0 Hz) to be used in the calculation. The red dashed lines show the non-linear curve fit of the experimental data to the appropriate 1:1 binding equation.

It was observed that the signals of H(2), H(3) and H(5) were shifted to higher fields upon the addition of **3**. These changes were taken as evidence that π-π donor-acceptor interactions between the aromatic ring of the anion and the 2,6-di(1H-imidazol-1-yl) pyridine fragments on

$\mathbf{1}^{4+}$ are involved in complex formation (stoichiometry inferred as 1:1 (host: guest) based on the Job plots; *vide supra*).

COSY and NOESY NMR spectroscopic studies were carried out in an effort to elucidate the nature of the host-guest interactions between macrocycle $\mathbf{1}^{4+}$ and **3** in D_2O (Figures S26 and S27). In the NOESY spectra, correlations between H(2, 4, 5 or 6) and H(3a), H(4 or 6) and H(3b), H(2) and H(3c) were observed. The spectra are consistent with the threaded binding mode proposed in the main text.

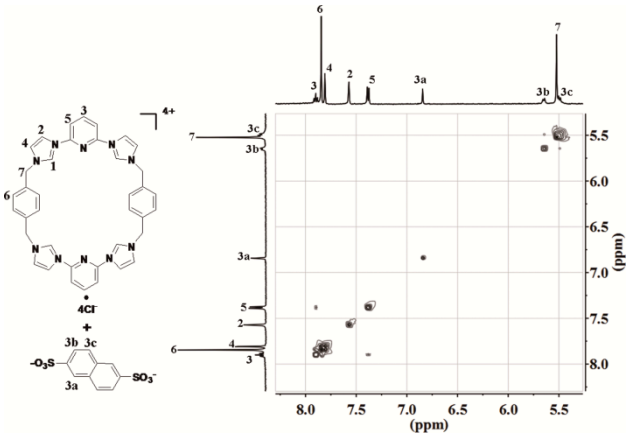

Figure S26. Full view of the 600 MHz COSY NMR spectrum of $\mathbf{1}^{4+}$•$4Cl^-$ (2.50 mM) recorded in D_2O at 300K in the presence of 1 molar equiv. of **3** and 2 molar equiv. of NaOH.

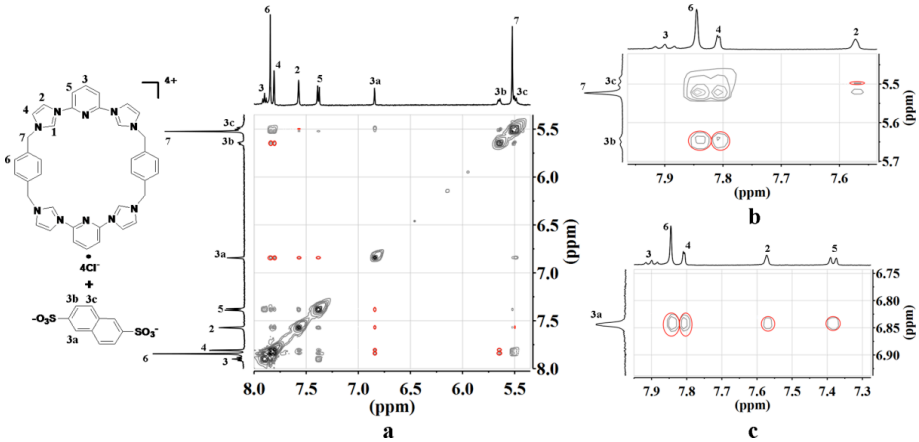

Figure S27. Full view of the 600 MHz NOESY NMR spectra of $\mathbf{1}^{4+}$•$4Cl^-$ (2.50 mM) recorded in D_2O at 300K in the presence of 1 molar equiv. of **3** and 2 molar equiv. of NaOH.

A 1D NOESY spectroscopic study between macrocycle $\mathbf{1}^{4+}$ and **3** was also carried out; it confirmed the correlated signal observed in the 2D NOESY spectrum (*e.g.*, the correlations between protons H(2, 4 or 6) and H(4a)). As such, this measurement provided greater detail regarding the correlations (*cf.* Figure S28).

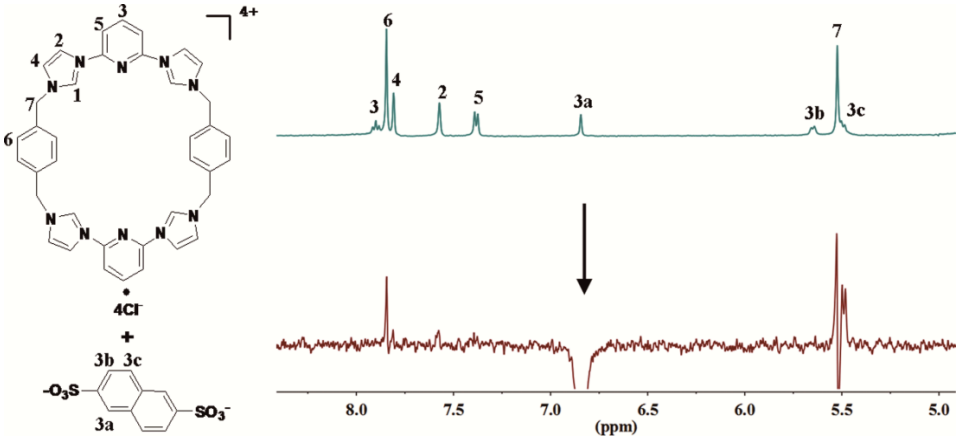

Figure S28. Expansion of the 1D ^{1}H NMR spectrum (top) and the corresponding selective 1D NOE NMR spectrum, which was obtained through irradiation at the frequency of H(3a) (bottom) of $\mathbf{1}^{4+}\cdot 4Cl^{-}$ (2.50 mM) recorded in D_2O at 300 K in the presence of 1 molar equiv. of **3** in the presence of 2 molar equiv. of NaOH (relative to **3**) (600 MHz).

Solution binding studies and characterization of the host-guest complex formed between 1^{4+} and the biphenyl-4,4′-disulfonate dianion (4):

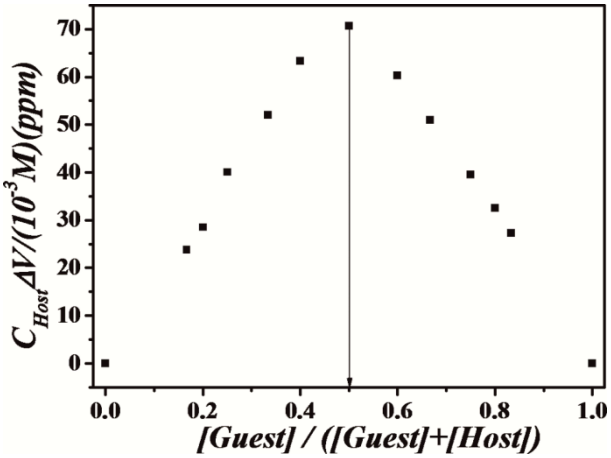

Figure S29. ^{1}H NMR Job-plots (600 MHz) corresponding to the binding between $\mathbf{1}^{4+}\bullet 4Cl^{-}$ and **4** ([host] + [guest] = 1×10^{-3} M) in D_2O. The maximum value of y (defined as the product of

chemical shift change value of H(3) on $\mathbf{1}^{4+}$ and the corresponding host concentration (i.e., [$\mathbf{1}^{4+}$]) was found at 0.5, a finding consistent with a 1:1 (host: guest) binding stoichiometry.[9]

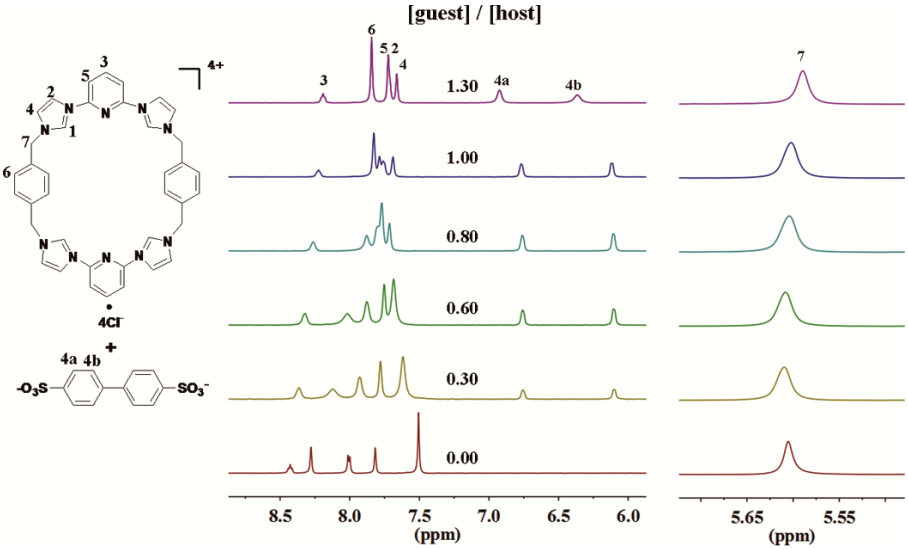

Figure S30. ^{1}H NMR spectroscopic titration of $\mathbf{1}^{4+}$•4Cl^{-} (5.00×10^{-4} M) with **4** in the presence of 2 molar equiv. of NaOH (relative to **4**). The spectra were recorded in D_2O at 300K and at 600 MHz.

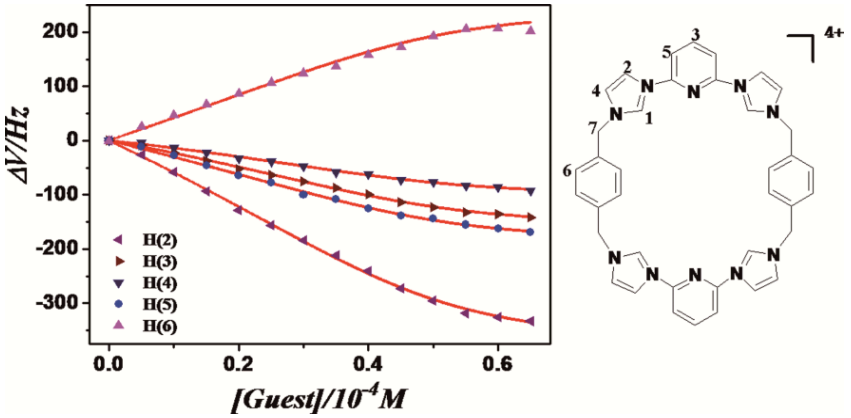

Figure S31. ^{1}H NMR binding isotherms corresponding to the interaction between $\mathbf{1}^{4+}$•4Cl^{-} and **4** in D_2O at 300K. The peak splitting technique *via* Gaussian functions was used for peak chemical shift confirmation.[11] The chemical shift changes of H(2), H(3), H(4), H(5) and H(6) on $\mathbf{1}^{4+}$ were used for the calculation of K_1 ($(3.5 \pm 0.2) \times 10^4$ M^{-1}) using the Hyperquad 2003 program.[10] The chemical shift changes in the signal corresponding to H(7) proved too small (less than 10.0 Hz) to be used in the calculation. The red dashed lines show the non-linear curve fit of the experimental data to the appropriate 1:1 binding equation.

It was observed that the signals of H(2), H(3), H(4) and H(5) were shifted to higher field upon the addition of **4**. These changes provide evidence that π-π donor-acceptor interactions between the aromatic ring of the anion and the 2,6-di(1H-imidazol-1-yl) pyridine fragments on $\mathbf{1}^{4+}$ are involved in complex formation (stoichiometry inferred as 1:1 (host: guest) based on the Job plot analysis; *vide supra*).

COSY and NOESY NMR spectroscopic studies were carried out in an effort to elucidate the nature of the host-guest interactions between macrocycle $\mathbf{1}^{4+}$ and **4** in D_2O (Figures S32 and S33). Correlations between H(2, 5, or 6) and H(4a, 4b), H(4) and H(4a, 4b) were observed. The spectra are consistent with the threaded binding mode shown in Scheme 1 of the main text (*cf.* also Figure S33).

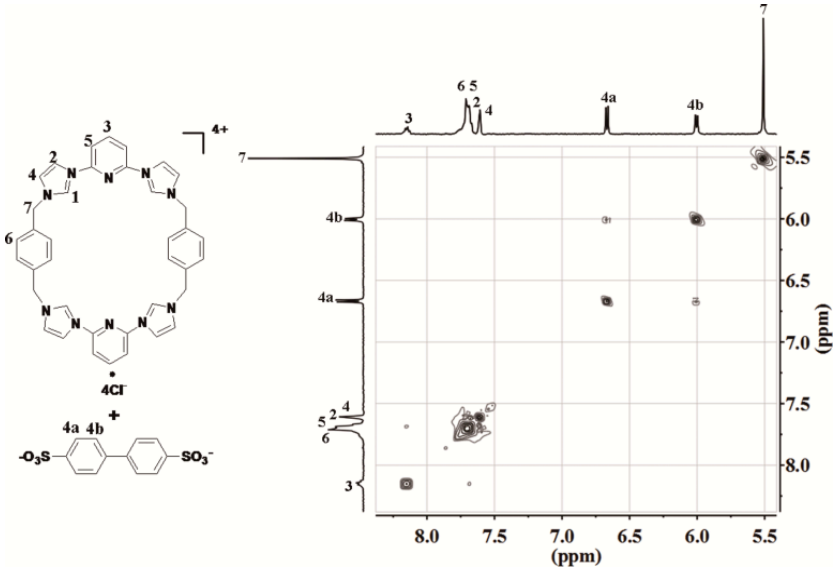

Figure S32. Full views of the 600 MHz COSY NMR spectra of $\mathbf{1}^{4+}$•$4Cl^-$ (2.50 mM) recorded in the presence of 1 molar equiv. **4** and 2 molar equiv. of NaOH in D_2O at 300K.

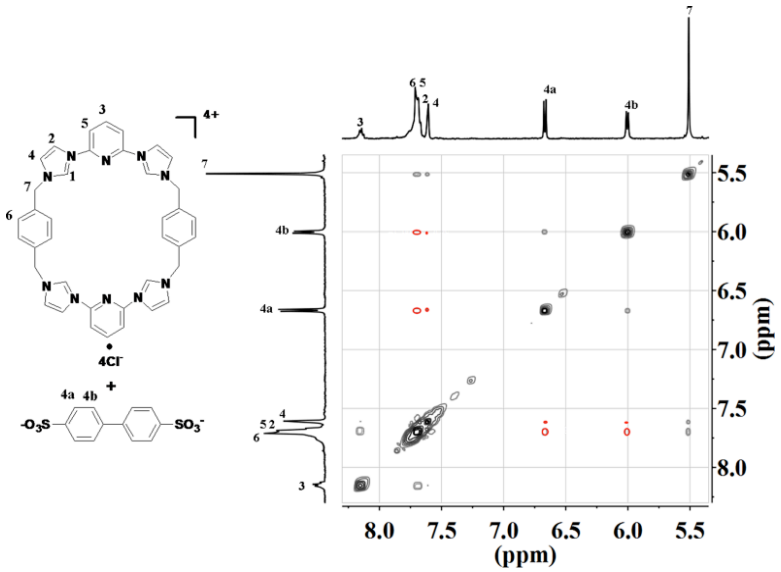

Figure S33. Full view of the 600 MHz NOESY NMR spectra of $\mathbf{1}^{4+}$•4Cl$^-$ (2.50 mM) recorded in the presence of 1 molar equiv. of **4** and 2 molar equiv. of NaOH in D_2O at 300K.

A 1D NOESY spectroscopic study involving a mixture of macrocycle $\mathbf{1}^{4+}$ and **4** was also carried out. As can be seen from an inspection of Figure S34, this analysis served to confirm the correlation observed in the 2D NOESY spectrum (*e.g.*, the correlations between protons H(2, 5 or 6) and H(4a, 4b)).

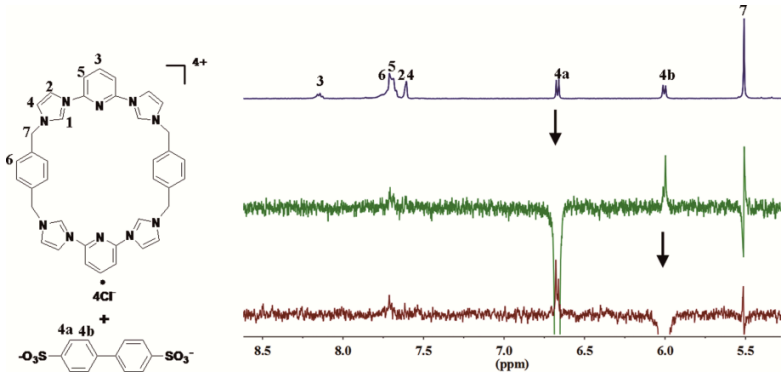

Figure S34. Expansion of the 1D ^{1}H NMR spectrum (top) and the corresponding selective 1D NOESY NMR spectrum, which was obtained through irradiation at the frequency of H(4a) (middle) and H(4b) (bottom) of $\mathbf{1}^{4+}\cdot$4Cl$^-$ (2.50 mM) recorded in the presence of 1 molar equiv. of **4** and 2 molar equiv. of NaOH in D_2O at 300 K (600 MHz).

Again, compared with $\mathbf{1}^{4+}\cdot 4PF_6^-$, the UV-vis spectrum of complex $[\mathbf{1}^{4+}\bullet\mathbf{n}]^{2+}$ (**n** = **2**, **3**, or **4**) was characterized by a small red shift. However, no charge-charge transfer band was observed in the long wavelength spectral region.

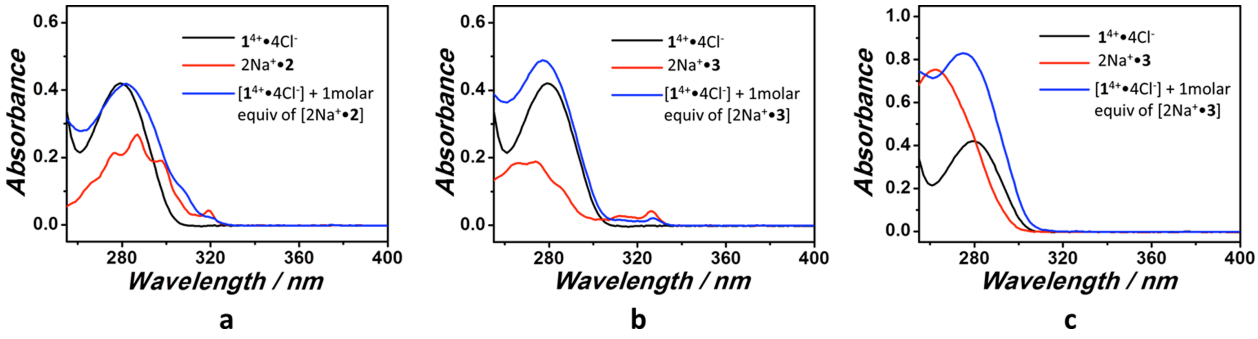

Figure S35. UV-vis spectra of $\mathbf{1}^{4+}\cdot 4Cl^-$ (6.00×10^{-5} M), $2Na^+\cdot\mathbf{n}$ (6.00×10^{-5} mM), and $\mathbf{1}^{4+}\cdot 4Cl^-$ (6.00×10^{-5} M) recorded in water in the presence of 1 molar equiv. of **2** (a), **3 (b), or 4 (c)**.

The titrations between $\mathbf{1}^{4+}$ and guests **3** or **4** carried out in [D_6]DMSO and D_2O were compared. The chemical shift changes of H(2, 3, or 5) on $\mathbf{1}^{4+}$ in D_2O is larger than what was observed in [D_6]DMSO under analogous titration conditions (Figure S36). This leads us to suggest that the π-π donor-acceptor interactions are enhanced in aqueous milieus.

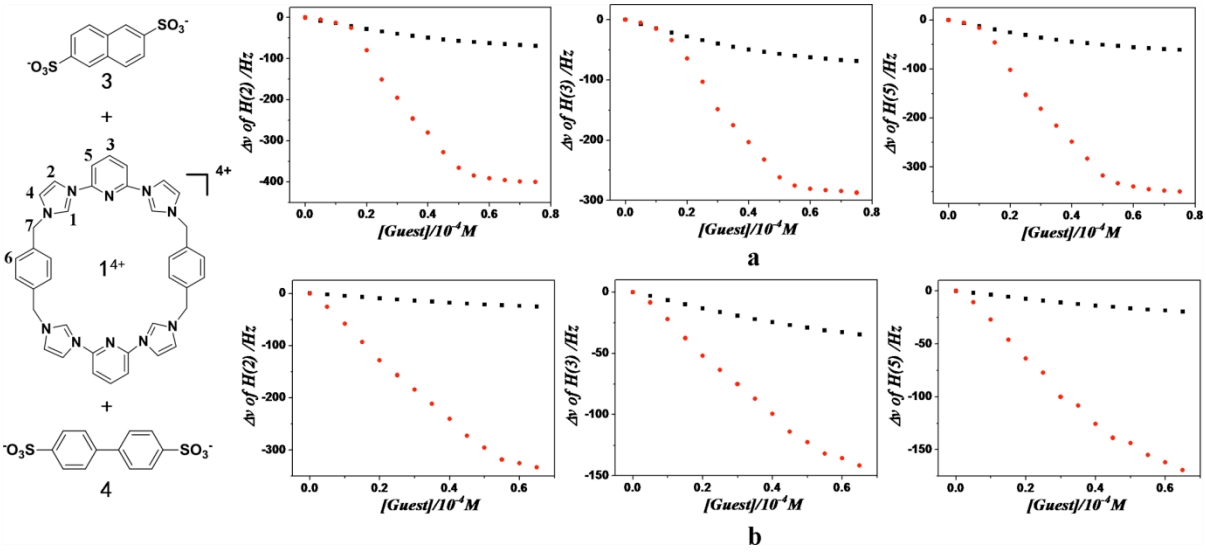

Figure S36. Comparison of chemical shift changes of H(2, 3, or 5) on $\mathbf{1}^{4+}$ recorded upon adding guests **3** (a) or **4** (b) to $\mathbf{1}^{4+}$ (5.00×10^{-4} M) in [D_6]DMSO or D_2O solution (indicated with "■" or "●", respectively).

All the solution phase results are summarized in Table S2 below. The greater values of the calculated association constants (*K*a) obtained in D_2O support the notion that pseudorotaxanes $[\mathbf{1}^{4+}\bullet\mathbf{3}]^{2+}$ and $[\mathbf{1}^{4+}\bullet\mathbf{4}]^{2+}$ are formed more effectively in water (D_2O) than organic media ([D_6]DMSO).

Table S2. Summary of solution state studies of the complex formation between $\mathbf{1}^{4+}$ and **2**, **3**, or **4**.

Host	Solvent	Guest	Stoichio-metry / (H:G)	Equilibrium	Association constants K_a	Binding mode
$\mathbf{1}^{4+}\bullet 4PF_6^-$	[D_6] DMSO	$2TMA^+\bullet$**2**	1:1	**[H] + [G]** $\overset{Ka}{\rightleftharpoons}$ **[H·G]**	$(1.0 \pm 0.1) \times 10^3$ M^{-1}	"outside" binding
		$2TMA^+\bullet$**3**	1:1	**[H] + [G]** $\overset{Ka}{\rightleftharpoons}$ **[H·G]**	$(1.6 \pm 0.1) \times 10^4$ M^{-1}	pseudo-rotaxane
		$2TMA^+\bullet$**4**	1:1	**[H] + [G]** $\overset{Ka}{\rightleftharpoons}$ **[H·G]**	$(3.0 \pm 0.2) \times 10^3$ M^{-1}	pseudo-rotaxane
$\mathbf{1}^{4+}\bullet 4Cl^-$	D_2O	$2Na^+\bullet$**3**	1:1	**[H] + [G]** $\overset{Ka}{\rightleftharpoons}$ **[H·G]**	$(3.4 \pm 0.2) \times 10^5$ M^{-1}	pseudo-rotaxane
		$2Na^+\bullet$**4**	1:1	**[H] + [G]** $\overset{Ka}{\rightleftharpoons}$ **[H·G]**	$(3.5 \pm 0.2) \times 10^4$ M^{-1}	pseudo-rotaxane

Section S5: Single crystal X-ray analysis of the complexes

Table S3. X-ray crystallographic data comparison of [$\mathbf{1}^{4+}$•$\mathbf{2}_2$•6H_2O], [$\mathbf{1}^{4+}$•$\mathbf{2}_2$•14H_2O], [$\mathbf{1}^{4+}$•$\mathbf{3}_2$•7.5H_2O], [$\mathbf{1}^{4+}$•$\mathbf{4}_2$•DMF•5.5H_2O], [$\mathbf{1}^{4+}$•$\mathbf{4}_2$•DMF•6H_2O] and [$\mathbf{1}^{4+}$•$\mathbf{4}_2$•9.5H_2O].

	$\mathbf{1}^{4+}$•$\mathbf{2}_2$•6H_2O	$\mathbf{1}^{4+}$•$\mathbf{2}_2$•14H_2O	$\mathbf{1}^{4+}$•$\mathbf{3}_2$•7.5H_2O
CCDC No.	1012717	1012718	1012719
description	needle	plate	prism
color	colorless	colorless	colorless
From solution	water/acetonitrile /DMF	water/acetonitrile /DMF	water/acetonitrile /DMF
empirical formula	C_{58} H_{58} N_{10} O_{18} S_4	C_{58} H_{74} N_{10} O_{26} S_4	C_{62} H_{60} N_{10} O_{20} S_4
Mr	1311.38	1455.51	1338.41
crystal size (mm^3)	0.26 × 0.14 × 0.09	0.30 × 0.20 × 0.04	0.22 × 0.14 × 0.08
crystal system	Triclinic	Triclinic	Triclinic
space group	P-1	P-1	P-1
a [Å]	7.8554(16)	10.5682(10)	12.2027(15)
b [Å]	13.428(3)	12.4098(10)	13.5862(16)
c [Å]	14.296(3)	13.8043(16)	19.851(2)
α [deg]	74.64(3)	70.117(2)	72.658(3)
β [deg]	83.39(3)	82.636(3)	78.079(3)
γ [deg]	82.18(3)	85.850(2)	72.902(3)
V/ [$Å^3$]	1435.7(5)	1687.7(3)	2977.0(6)
d/[g/cm^3]	1.517	1.432	1.493
Z	1	1	2
T [K]	173(2)	153(2)	153(2)
R1, wR2 $I > 2ó(I)$	0.0967 0.1691	0.0701 0.1592	0.0952 0.1967
R1, wR2 (all data)	0.1297 0.1932	0.0909 0.1793	0.1738 0.2351
quality of fit	0.906	1.019	1.017

	$\mathbf{1}^{4+}$•$\mathbf{4}_2$•DMF•5.5H_2O	$\mathbf{1}^{4+}$•$\mathbf{4}_2$•DMF•6H_2O	$\mathbf{1}^{4+}$•$\mathbf{4}_2$•9.5H_2O
CCDC No.	1012720	1012721	1012722
description	prism	prism	prism
color	colorless	colorless	colorless
From solution	water/acetonitrile /DMF	water/ DMF	water/DMF
empirical formula	C_{65} H_{68} N_{11} $O_{18.50}$ S_4	C_{65} H_{69} N_{11} O_{19} S_4	C_{65} H_{57} N_{11} $O_{18.50}$ S_4
Mr	1427.54	1436.55	1426.51
crystal size (mm^3)	0.57 × 0.18 × 0.06	0.25 × 0.21 × 0.07	0.23× 0.13 × 0.07
crystal system	Triclinic	Triclinic	Triclinic
space group	P-1	P-1	P-1
a [Å]	14.085(3)	13.900(3)	14.166(3)
b [Å]	16.457(3)	16.237(3)	16.380(3)
c [Å]	16.585(3)	16.444(3)	18.029(3)
α [deg]	80.08(3)	79.98(3)	103.04(3)
β [deg]	66.96(3)	66.84(3)	109.53(3)
γ [deg]	72.44(3)	73.12(3)	98.05(3)
V/ [$Å^3$]	3366.4(12)	3257.7(11)	3733.8(13)
d/[g/cm^3]	1.408	1.465	1.269
Z	2	2	2
T [K]	223(2)	173(2)	223(2)
R1, wR2 $I > 2ó(I)$	0.0798 0.1617	0.0866 0.2146	0.0984 0.1985
R1, wR2 (all data)	0.1651 0.2144	0.1209 0.2397	0.1912 0.2439
quality of fit	1.033	1.013	1.043

Single-crystal analysis for structure 1^{4+}•2_2•$6H_2O$:

Addition of 5 molar equiv. of 1,5-naphthalene disulfonate dianion (**2**; tetramethylammonium (TMA^+) salt; 1 mL, 10.3 mM) in water to a solution of 5 mg $\mathbf{1}^{4+}$•4PF_6^- (2.8 mmol) in 1.5 mL of acetonitrile/water/DMF (1/1/1, v/v/v), and subsequent crystal growth from an acetonitrile/water/DMF mixed solvent system by slow evaporation, produced two independent single crystals corresponding to $\mathbf{1}^{4+}$•$\mathbf{2}_2$•6H_2O and $\mathbf{1}^{4+}$•$\mathbf{2}_2$•14H_2O. These crystals were used to

determine the structure of the resulting complexes *via* X-ray diffraction analysis. In the single crystal structure of $\mathbf{1}^{4+}\bullet\mathbf{2}_2\bullet 6H_2O$, the complex formed between $\mathbf{1}^{4+}$ and the neighboring guest anions was found to adopt two different "outside" binding modes, which were found to bind the 1,5-naphthalene disulfonate dianions at the "top" of their respective central cavities (Figure S37 and S39). These findings lead us to suggest that the complex is predominantly stabilized by C-H···anion intermolecular hydrogen bonding and π-π donor-acceptor interactions.

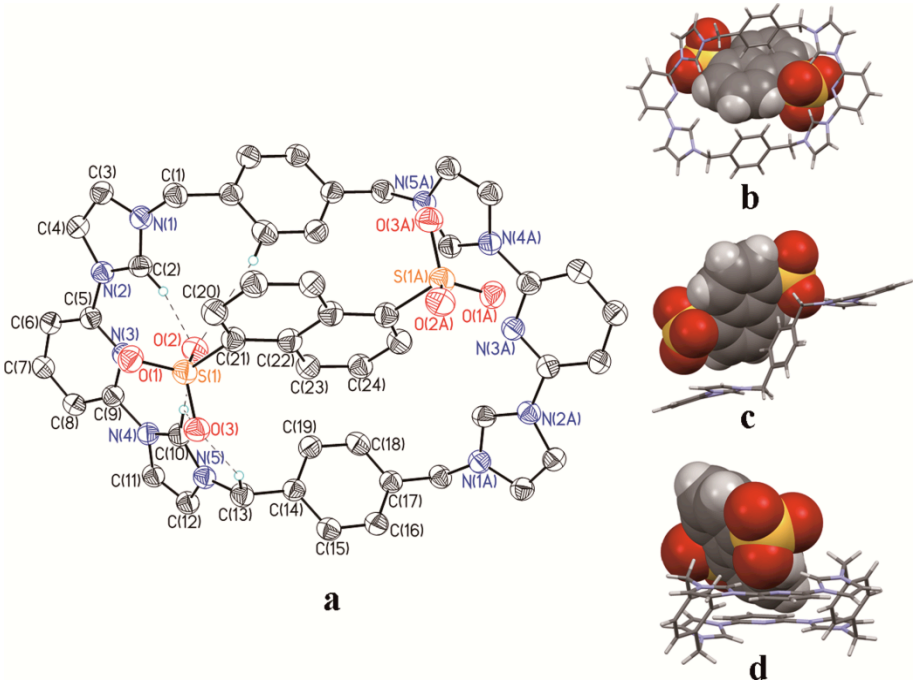

Figure S37. (a) Top view showing the ellipsoid form, and (b) the top view, (c) side view and (d) front view showing the stick form of the "partial chair" conformation of $\mathbf{1}^{4+}$ with a co-bound 1,5-naphthalene disulfonate anion present in $\mathbf{1}^{4+}\bullet\mathbf{2}_2\bullet 6H_2O$. Displacement ellipsoids are scaled to the 25% probability level. Some or all of the counter anions, solvent molecules and hydrogen atoms have been omitted for clarity. Selected bond distances and angles between $\mathbf{1}^{4+}$ and the 1,5-naphthalene disulfonate anion are as follows. Intermolecular hydrogen bonds: Selected interatomic distances [Å]: C(2)…O(2) 3.032(8), C(10)…O(2) 3.137(8). C(10)…O(3) 3.512(8), C(13)…O(3) 3.305(9), C(18)…O(2) 3.512(7). Selected interatomic angles: C(2)-H(2A)…O(2) 153.5(4)º, C(10)-H(10A)…O(2) 177.5(4)º, C(10)-H(10A)…O(3) 123.8(4)º, C(13)-H(13B)…O(3) 158.7(4)º, C(18)-H(18A)…O(2) 140.8(4)º. Possible π-π donor-acceptor interactions are inferred

from the interatomic distances [Å]: N(3)…O(2) 3.408(6), C(8)…O(1) 3.248(7), C(11)…O(1) 3.431(8), C(11)…O(3) 3.430(8), C(20)…C(10) 3.701(8), C(20)…N(4) 3.755(7), C(22)…C(18) 3.572(8), C(23)…C(18) 3.736(9), C(23)…C(19) 3.769(8).

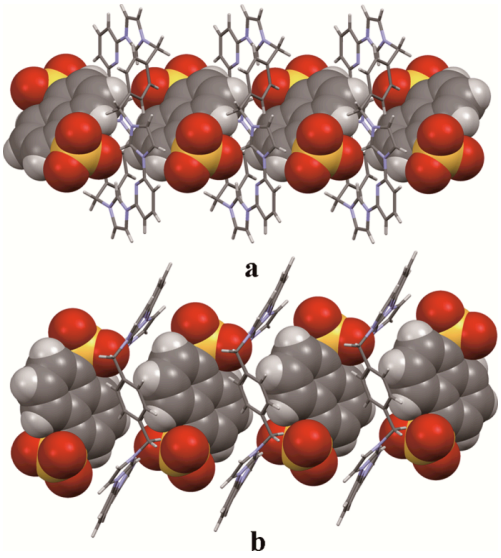

Figure S38. Extended single crystal packing structure showing formation of the 1D self-assembled system in the structure of $\mathbf{1}^{4+}$•$\mathbf{2}_2$•$6H_2O$ as shown from; (a) top and (b) side views.

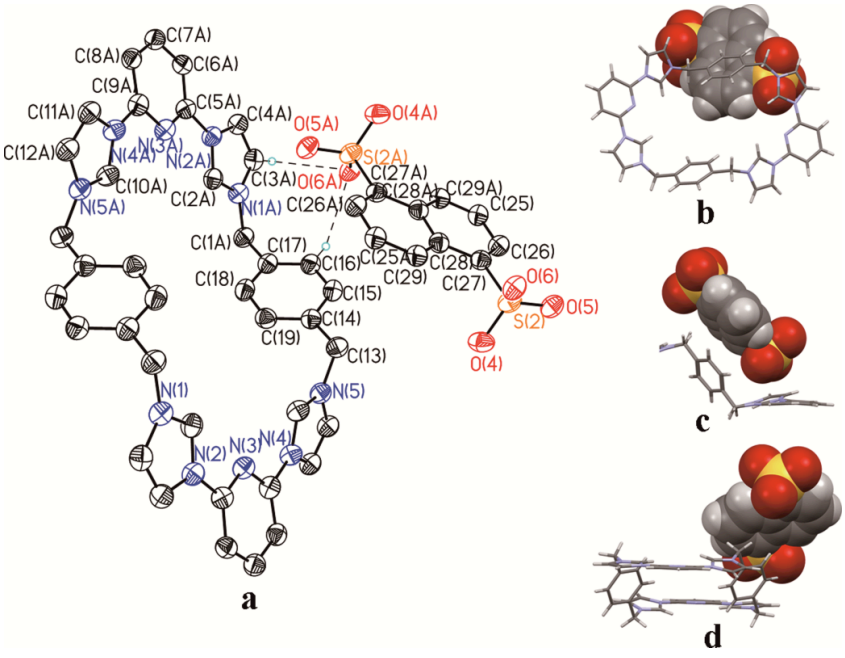

Figure S39. (a) Top view showing the ellipsoid form, and (b) the top view, (c) side view, and (d) front view showing the stick form of the "partial chair" conformation of $\mathbf{1}^{4+}$ with a co-bound

1,5-naphthalene disulfonate anion present in $\mathbf{1}^{4+}\bullet\mathbf{2}_2\bullet 6H_2O$. Displacement ellipsoids are scaled to the 25% probability level. Some or all of the counter anions, solvent molecules and hydrogen atoms have been omitted for clarity. Selected bond distances between $\mathbf{1}^{4+}$ and the 1,5-naphthalene disulfonate anion are as follows, with possible π-π donor-acceptor interactions inferred from these structural parameters [Å]: C(3)...O(6) 3.246(7), C(2)...O(5) 3.288(7), C(3)...O(5) 3.287(9), C(4)...O(5) 3.228(8), N(1)...O(5) 3.329(7), N(1)...O(6) 3.656(6), N(2)...O(5) 3.228(6), C(25)...C(15) 3.68(1), C(26)...C(15) 3.467(9), C(26)...C(16) 3.80(1), C(27)...C(15) 3.472(9), C(27)...C(16) 3.571(9), C(28)...C(15) 3.700(8).

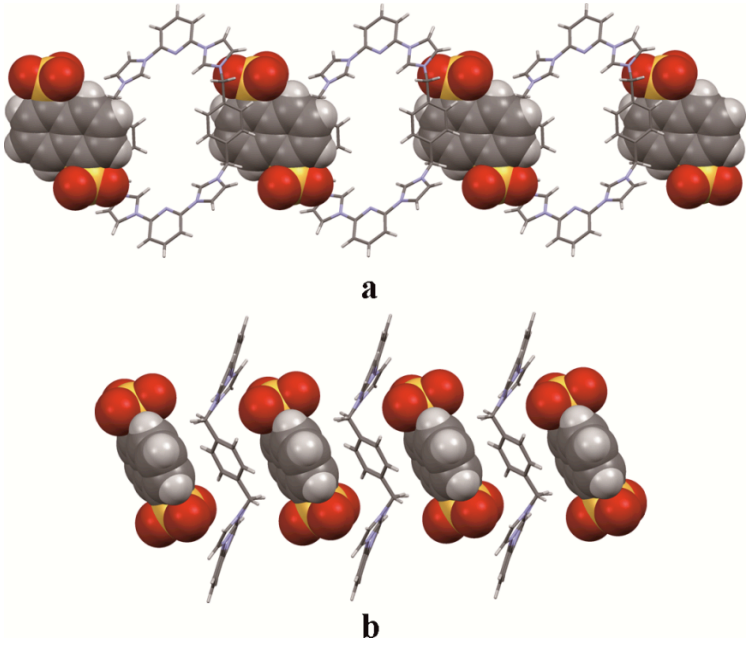

Figure S40. Extended single crystal packing structure showing formation of the 1D self-assembled system present in the structure of $\mathbf{1}^{4+}\bullet\mathbf{2}_2\bullet 6H_2O$ as viewed from the (a) top and (b) side perspectives.

Single-crystal analysis for structure $1^{4+}\bullet 2_2\bullet 14H_2O$:

The complex formed between the macrocyclic host and the neighboring guest anions was found to adopt two different "outside" binding modes (Figure S41 and 42). These findings lead us to suggest that the complex is predominantly stabilized by π···π donor-acceptor interactions, as well as weak intermolecular hydrogen bonds.

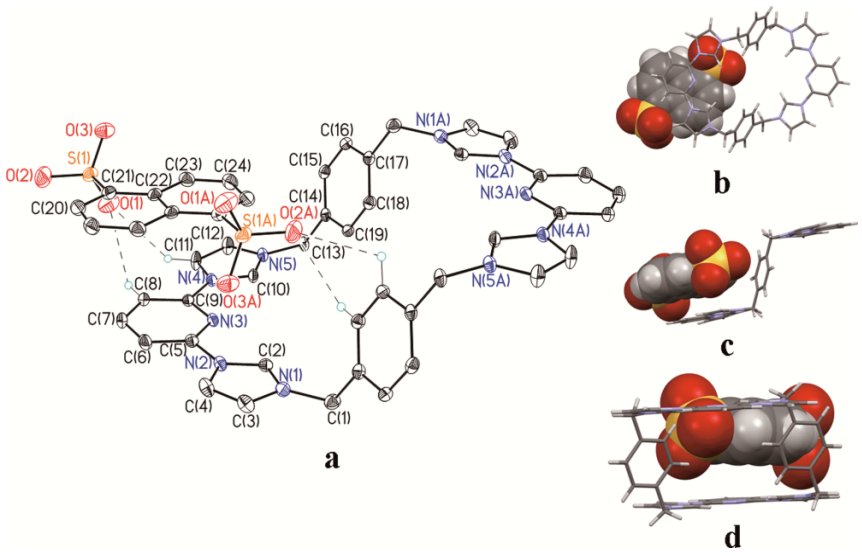

Figure S41. (a) Top view showing the ellipsoid form, and (b) the top view, (c) side and (d) front view showing the first of two "outer" binding modes present in the structure of $\mathbf{1}^{4+}\bullet\mathbf{2}_2\bullet 14H_2O$. Displacement ellipsoids are scaled to the 25% probability level. Some or all of the counter anions, solvent molecules and hydrogen atoms have been omitted for clarity. Selected bond distances between $\mathbf{1}^{4+}$ and the 1,5-naphthalene disulfonate anion **2** are as follows. Possible intermolecular hydrogen bonding interactions were inferred from these structural parameters [Å]: C(8)...O(1) 3.487(5), C(11)...O(1) 3.394(6), C(18A)...O(2A) 3.160(5), C(19A)...O(2A) 3.381(6). Selected interatomic angles: C(8)-H(8A)…O(1) 136.9(3)º, C(11)-H(11A)…O(1) 126.4(3)º, C(18A)-H(18A)…O(2) 125.5(3)º, C(19A)-H(19A)…O(2) 109.4(3)º. The possible π-π donor-acceptor interactions were inferred from the following selected interatomic distances [Å]: N(1)...O(3) 3.417(4), N(2)...O(3) 2.807(5), N(3)...O(3) 3.762(5), C(20)...C(10) 3.746(6), C(21)...N(3) 3.654(5), C(22)...N(3) 3.789(5), C(22)...C(8) 3.751(6), C(22)...C(9) 3.706(6), C(23)...C(6) 3.594(5), C(23)...C(7) 3.682(6), C(24)...C(7) 3.618(6). C(20A)...C(7) 3.678(5), C(21A)...C(8) 3.536(5), C(22A)...C(8) 3.444(5), C(22A)...C(9) 3.600(5), C(23A)...C(9) 3.694(5), C(23A)...N(4) 3.484(5), C(23A)...C(11) 3.595(7), C(24A)...N(4) 3.486(6), C(24A)...N(5) 3.743(6), C(24A)...C(10) 3.431(6).

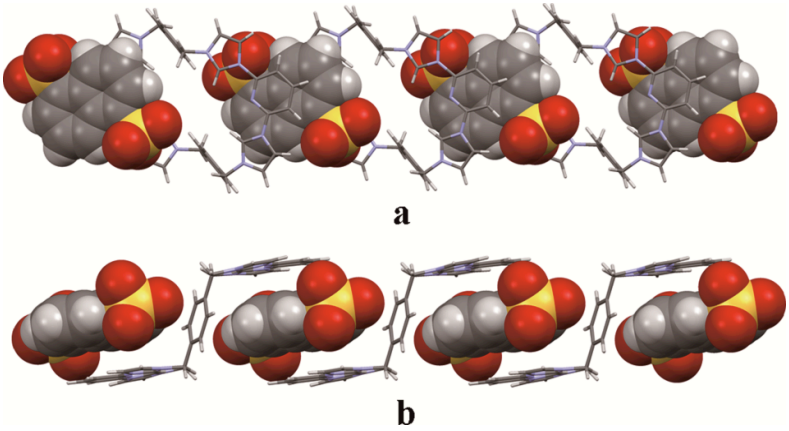

Figure S42. Extended single crystal packing structure showing formation of the 1D self-assembled system in the structure of $\mathbf{1}^{4+}\bullet\mathbf{2}_2\bullet 14H_2O$ as seen from (a) the top and (b) side perpectives.

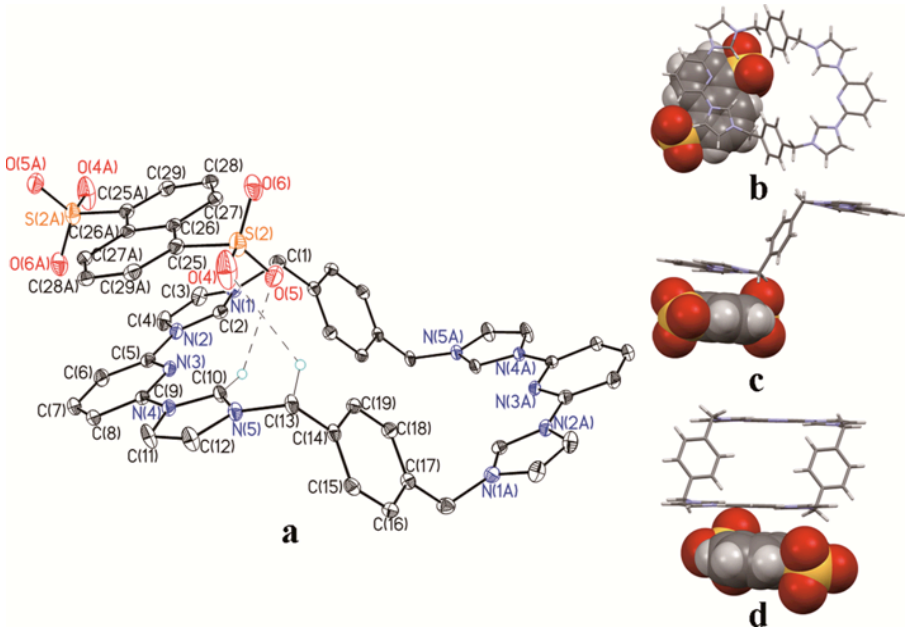

Figure S43. (a) Top view showing the ellipsoid form, and (b) the top, (c) side, and (d) front views showing the second of two "outer" binding modes present in the structure of $\mathbf{1}^{4+}\bullet\mathbf{2}_2\bullet 14H_2O$. Displacement ellipsoids are scaled to the 25% probability level. Some or all of the counter anions, solvent molecules and hydrogen atoms have been omitted for clarity. Selected bond distances between $\mathbf{1}^{4+}$ and the 1,5-naphthalene disulfonate anion are as follows with possible π-π donor-acceptor interactions inferred from these selected interatomic distances [Å]: N(2)...O(6) 3.738(5), N(5)...O(4) 3.413(6), N(5)...O(5) 3.795(5), C(4)...O(10) 3.418(6), C(4)...O(6A)

3.356(7), C(6)...O(6A) 3.484(5). C(25)...N(3) 3.590(5), C(26)...N(2) 3.794(5), C(26)...N(3) 3.739(4), C(26)...C(2) 3.487(6), C(27)...N(1) 3.765(5), C(27)...C(2) 3.455(5), C(28)...N(1) 3.392(5), C(28)...C(2) 3.544(5), C(29)...N(3) 3.489(5), C(29)...N(4) 3.459(4), C(29)...C(9) 3.461(5), C(29)...C(10) 3.677(5), C(25A)...N(2) 3.538(4), C(25A)...C(2) 3.713(6), C(25A)...C(4) 3.632(6), C(26A)...N(2) 3.464(5), C(26A)...N(3) 3.748(4), C(26A)...C(2) 3.625(6), C(26A)...C(5) 3.549(5), C(27A)...N(3) 3.603(5), C(27A)...C(5) 3.450(6), C(27A)...C(6) 3.659(5), C(28A)...N(3) 3.484(5), C(28A)...C(5) 3.782(6), C(28A)...C(8) 3.645(5), C(28A)...C(9) 3.383(5), C(29A)...N(1) 3.447(6), C(29A)...C(2) 3.661(5), C(29A)...C(3) 3.583(6).

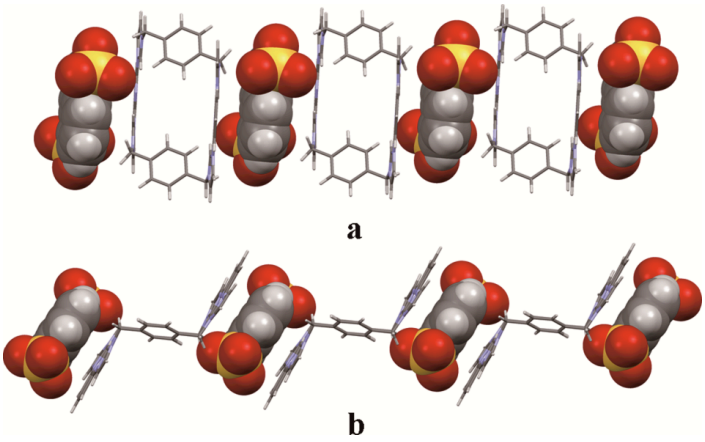

Figure S44. Extended single crystal packing structure showing formation of the 1D self-assembled system present in the pseudorotaxane structure of $\mathbf{1}^{4+}\bullet\mathbf{2}_2\bullet 14H_2O$ as shown from the (a) top and (b) side perspectives.

Single-crystal analysis for structure $1^{4+}\bullet 3_2\bullet 7.5H_2O$:

The addition of 1 or 5 molar equiv of 2,6-naphthalene disulfonate dianion (tetramethylammonium hydroxide ($TMA^+\bullet OH^-$) salt) to a solution of $\mathbf{1}^{4+}\bullet 4PF_6^-$, and subsequent crystal growth from an acetonitrile/water/DMF mixed solvent system by slow evaporation, produced single crystals of $\mathbf{1}^{4+}\bullet\mathbf{3}_2\bullet 7.5H_2O$ that were used to determine the structure of the resulting complex *via* X-ray diffraction analysis. This analysis revealed the formation of a pseudorotaxane structure stabilized through multiple intermolecular hydrogen bonding and π···π

donor-acceptor interactions (Figure S45). A 1D self-assembled system with apparent donor-acceptor-donor (DAD) interactions is also seen in the structure (Figure S46).

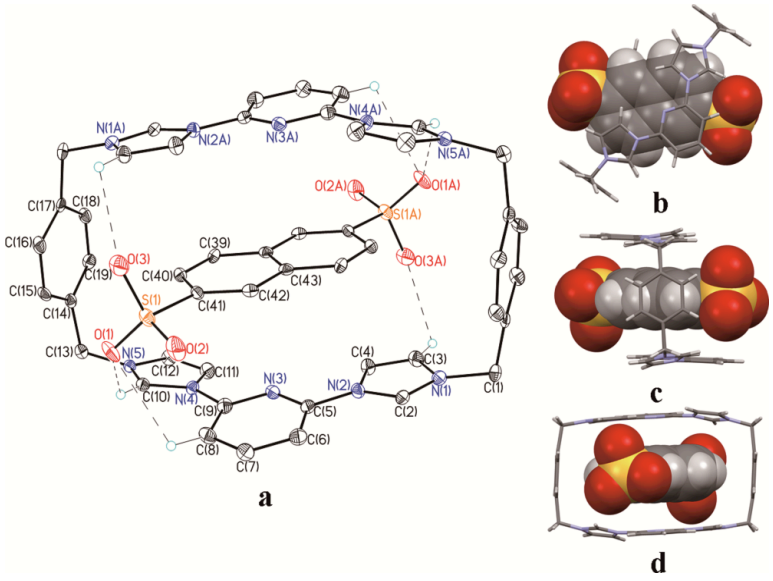

Figure S45. Single crystal X-ray structure of the pseudorotaxane structure [$\mathbf{1}^{4+}$•$\mathbf{3}_2$•7.5H_2O] highlighting (a) the view of the pseudorotaxane complex [$\mathbf{1}^{4+}$•$\mathbf{3}$]$^{2+}$ present in [$\mathbf{1}^{4+}$•$\mathbf{3}_2$•7.5H_2O] and the atom labeling scheme. Also shown are top (b) and side views (c) and (d) of the pseudorotaxane structure. Displacement ellipsoids are scaled to the 25% probability level. Some or all of the counter anions, solvent molecules, and hydrogen atoms have been omitted for clarity. Possible intermolecular hydrogen bonding interactions were inferred from the following selected interatomic distances [Å]: C(3)...O(3) 3.28(1), C(8)...O(1) 3.370(8), C(10)...O(1) 3.35(1). Selected interatomic angles: C(3)-H(3A)…O(3) 121.2(5)º, C(8)-H(8A)…O(1) 108.4(5)º, C(10)-H(10A)…O(1) 129.5(4)º. Possible π-π donor-acceptor interactions were inferred from the following selected interatomic distances [Å]: C(4)...O(3) 3.65(1), C(7)...O(2) 3.573(8), C(8)...O(2) 3.695(9), C(39)...N(2) 3.389(8), C(39)...N(4) 3.609(8), C(39)...C(2) 3.677(9), C(39)...C(4) 3.557(9), C(39)...C(5) 3.72(1), C(39)...C(11) 3.640(9), C(40)...N(2) 3.728(9), C(40)...N(4) 3.370(8), C(40)...C(3) 3.468(9), C(40)...C(4) 3.411(9), C(40)...C(9) 3.615(9), C(40)...C(10) 3.395(9), C(41)...N(3) 3.782(8), C(41)...C(4) 3.67(1), C(41)...C(8) 3.63(1), C(41)...C(9) 3.458(9), C(42)...N(3) 3.542(7), C(42)...C(5) 3.566(9), C(42)...C(6) 3.78(1), C(42)...C(9) 3.668(9), C(43)...N(2A) 3.715(7), C(43)...C(5A) 3.55(1).

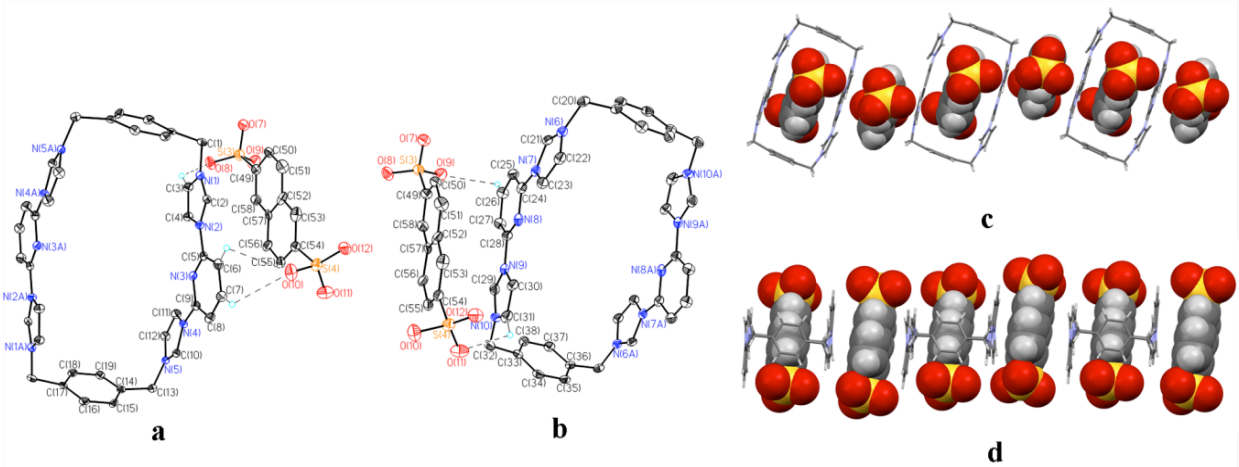

Figure S46. Extended single crystal packing structure showing formation of a 1D 'DAD' self-assembly complex. These figures show views designed to highlight the interaction between the two neighboring pseudorotaxane "monomer" units present in the complex [$\mathbf{1}^{4+}$•$\mathbf{3}_2$•7.5H_2O]. Views (a) and (b) show the atom labeling scheme of the complex containing only a molecule of **3** bound the outer periphery (the molecule of **3** that threads through $\mathbf{1}^{4+}$ has been removed for clarity). Also shown are side views (c) and (d) of the 1D 'DAD' self-assembled complex formed by interaction with neighboring pseudorotaxane units and bridged by molecules of **3**. From this structure it is presumed that the stabilizing interactions between these two units are predominantly π···π interactions as inferred from the following selected interatomic distances [Å]: C(49)...N(1) 3.48(2), C(49)...N(1) 3.42(2), C(50)...N(1) 3.50(1), C(51)...N(1) 3.63(1), C(51)...C(2) 3.72(1), C(52)...N(1) 3.74(2), C(52)...C(2) 3.43(2), C(54)...C(6) 3.46(2), C(55)...C(5) 3.46(2), C(55)...C(6) 3.30(2), C(55)...C(7) 3.64(2), C(56)...N(2) 3.43(2), C(56)...N(3) 3.70(2), C(56)...C(5) 3.37(2), C(56)...C(6) 3.73(2), C(57)...N(1) 3.73(1), C(57)...N(2) 3.40(2), C(57)...C(2) 3.49(2), C(57)...C(4) 3.63(2), C(58)...N(1) 3.59(1), C(58)...N(2) 3.71(1), C(58)...C(3) 3.36(2), C(58)...C(4) 3.42(1), C(25)...O(9) 3.68(1), C(27)...O(9) 3.56(1), C(49)...C(26) 3.76(2), C(49)...C(27) 3.79(2), C(50)...C(24) 3.69(1), C(51)...N(8) 3.69(1), C(52)...N(8) 3.72(2), C(53)...C(30) 3.67(2), C(54)...C(30) 3.55(2), C(54)...C(31) 3.60(2), C(55)...N(10) 3.59(2), C(55)...C(30) 3.61(2), C(55)...C(31) 3.39(2), C(56)...C(29) 3.51(2), C(56)...C(30) 3.77(2), C(56)...N(9) 3.56(2), C(56)...N(10) 3.66(2).

Single-crystal analysis for structures 1^{4+}•4_2•DMF•5.5H_2O and 1^{4+}•4_2•DMF•6H_2O:

Addition of 5 molar equiv. of biphenyl-4,4′-disulfonate dianion (**4**; tetramethyl- ammonium (TMA^+) salt) to a solution of $\mathbf{1}^{4+}$•4PF_6^-, and subsequent crystal growth from an acetonitrile/water/DMF mixed solvent system by slow evaporation, produced a single crystal of $\mathbf{1}^{4+}$•$\mathbf{4}_2$•DMF•5.5H_2O that was used to determine the structure of the resulting complex *via* X-ray diffraction analysis. Separately, a solution of $\mathbf{1}^{4+}$•4Cl^- (30.8 mM, 210 μL) in deionized water was added into a solution of the disulfonate dianion **4** (25 mM, 1300 μL, produced *in situ* by mixing the corresponding disulfonic acid and two molar equiv. of NaOH) in water. The white precipitate that resulted was collected and washed with 2 mL deionized water. This product was dissolved in a mixture of DMF and water (1:1, v/v), and then filtered to obtain a clear solution. The resulting solution was allowed to evaporate slowly giving diffraction grade single crystals of $\mathbf{1}^{4+}$•$\mathbf{4}_2$•DMF•6H_2O. As detailed in the main text, the structures of $\mathbf{1}^{4+}$•$\mathbf{4}_2$•DMF•6H_2O and $\mathbf{1}^{4+}$•$\mathbf{4}_2$•DMF•5.5H_2O] proved structurally similar.

As determined from the resulting single crystal X-ray structure of [$\mathbf{1}^{4+}$•$\mathbf{4}_2$•DMF•5.5H_2O], one molecule of **4** is inserted into the cavity of $\mathbf{1}^{4+}$ to form a pseudorotaxane complex (Figure S47). Pseudorotaxane [$\mathbf{1}^{4+}$•**4**]$^{2+}$ in the single crystal of [$\mathbf{1}^{4+}$•$\mathbf{4}_2$•DMF•6H_2O] is structurally similar to that observed in the single crystal of [$\mathbf{1}^{4+}$•$\mathbf{4}_2$•DMF•5.5H_2O].

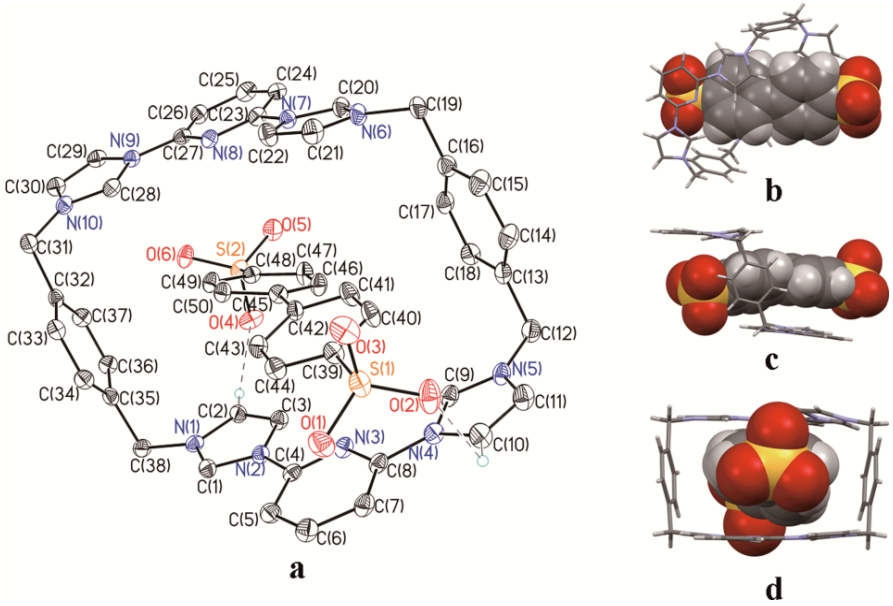

Figure S47. Single crystal X-ray structure of the pseudorotaxane structure $\mathbf{1}^{4+}\bullet\mathbf{4}_2\bullet$DMF$\bullet$5.5$H_2O$ highlighting (a) the pseudorotaxane complex $[\mathbf{1}^{4+}\bullet\mathbf{4}]^{2+}$ present in $[\mathbf{1}^{4+}\bullet\mathbf{4}_2\bullet$DMF$\bullet$5.5$H_2O]$ along with the atom labeling scheme. Also shown are top (b) and side views (c) and (d) of the pseudorotaxane structure. Displacement ellipsoids are scaled to the 25% probability level. Some or all of the counter anions, solvent molecules, and hydrogen atoms have been omitted for clarity. Possible intermolecular hydrogen bonding interactions were inferred based on the following selected interatomic distances [Å]: C(2)...O(4) 3.443(8), C(10)...O(2) 3.237(8). Selected interatomic angles: C(2)-H(2A)…O(4) 159.7(4)º, C(10)-H(10A)…O(2) 111.4(4)º. Possible π-π donor- acceptor interactions were inferred based on the following selected interatomic distances [Å]: C(7)...O(1) 3.624(8), N(8)...O(5) 3.487(6), C(23)...O(5) 3.524(8), C(24)...O(5) 3.704(7), C(25)...O(5) 3.742(8), C(26)...O(5) 3.652(7), C(27)...O(5) 3.524(6), N(8)...O(6) 3.487(7), N(9)...O(6) 2.956(6), N(10)...O(6) 3.588(6), C(27)...O(6) 3.171(7), C(28)...O(6) 3.010(6), C(29)...O(6) 3.525(6), C(36)...O(6) 3.54(1), C(37)...O(6) 3.220(9), C(39)...N(4) 3.756(7), C(39)...C(7) 3.654(9), C(39)...C(8) 3.568(8), C(40)...N(4) 3.437(7), C(40)...C(8) 3.699(9), C(40)...C(9) 3.680(9), C(40)...C(10) 3.667(8), C(41)...N(4) 3.707(7), C(41)...C(9) 3.560(8), C(42)...N(3) 3.476(7), C(43)...N(3) 3.465(7), C(43)...C(4) 3.448(8), C(44)...N(3) 3.768(8), C(44)...C(6) 3.731(9), C(44)...C(7) 3.674(8), C(44)...C(8) 3.649(8), C(45)...C(3) 3.495(9), C(46)...C(3) 3.52(1), C(46)...C(17) 3.66(1), C(46)...C(18) 3.77(1),

C(47)...C(3) 3.72(1), C(48)...N(8) 3.602(6), C(48)...C(2) 3.516(9), C(49)...N(8) 3.792(8), C(49)...C(2) 3.439(9), C(49)...C(28) 3.691(6), C(50)...C(2) 3.706(9), C(50)...C(3) 3.628(8).

As highlighted by Figure S48, a 1D self-assembled complex is present in the structures of $\mathbf{1}^{4+}$•$\mathbf{4}_2$•DMF•5.5H_2O and $\mathbf{1}^{4+}$•$\mathbf{4}_2$•DMF•6H_2O. These extended arrays are built up from individual pseudorotaxane units as well as bridging molecules of **4**. From the structural parameters, it is presumed that π-π donor-acceptor interactions constitute the main inter-complex stabilizing forces.

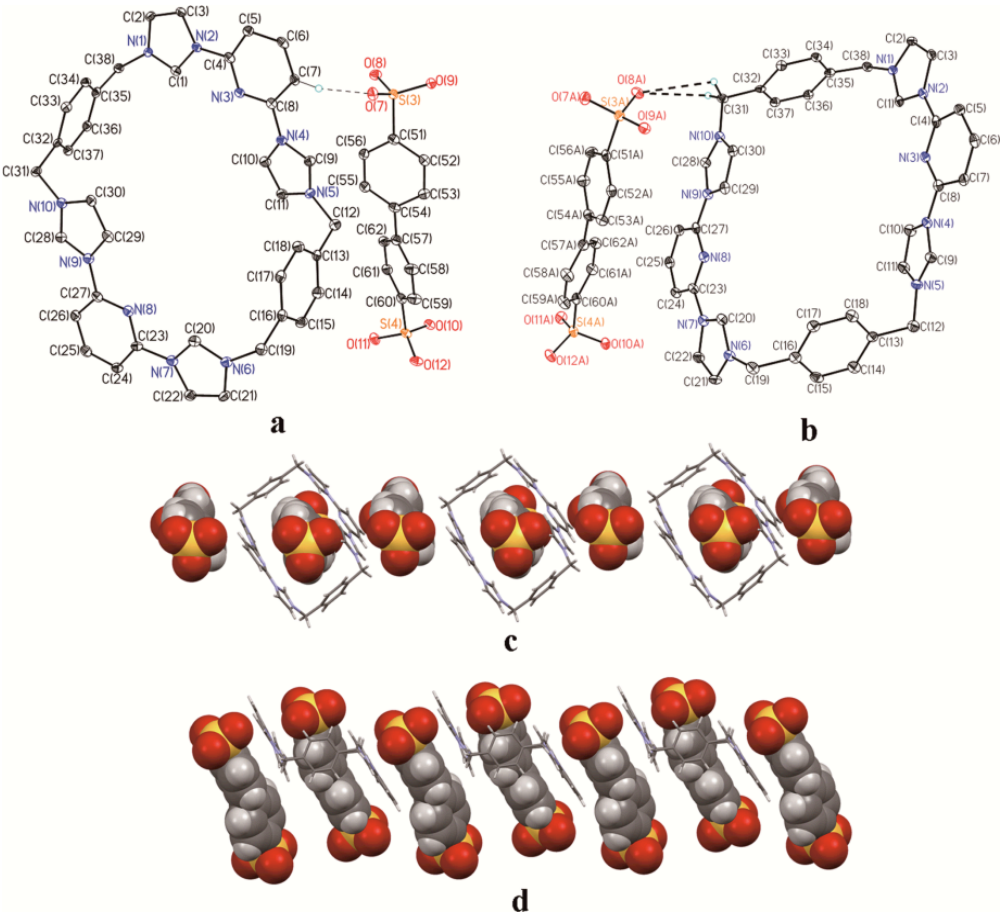

Figure S48. Extended single crystal packing structure showing the 1D 'DAD' self-assembled complex present in complex [$\mathbf{1}^{4+}$•$\mathbf{4}_2$•DMF•6H_2O]. Views (a) and (b) show the atom labeling scheme of the complex with the molecule of **4** bound the outer periphery (the threaded molecule of **4** has been removed for clarity), while views (c) and (d) show a side-on perspective of the 1D

'DAD' self-assembled complex. The presence of π···π interactions was inferred from the following selected interatomic distances [Å]: N(4)…O(7) 3.739(8), C(8)…O(7) 3.76(1), C(9)…O(7) 3.431(8), C(56)…N(5) 3.656(9), N(9)...O(9A) 3.669(7), N(10)...O(8A) 3.493(8), N(10)...O(9A) 3.154(6), C(28)...O(8A) 3.628(9), C(28)...O(9A) 3.420(7), C(29)...O(9A) 3.589(8), C(30)...O(9A) 3.282(8), C(51A)...C(28) 3.741(9), C(52A)...N(9) 3.566(8), C(52A)...C(26) 3.497(8), C(52A)...C(27) 3.493(9), C(52A)...C(28) 3.746(8), C(53A)...C(25) 3.427(9), C(53A)...C(26) 3.156(8), C(53A)...C(27) 3.546(9), C(54A)...C(25) 3.63(1), C(54A)...C(26) 3.539(9), C(57A)...C(25) 3.50(1), C(62A)...C(25) 3.63(1).

Single-crystal analysis for structure 1^{4+}•4_2•9.5H_2O:

The same method used to obtain the diffraction grade single crystals of complex **1**$^{4+}$•**4**$_2$•DMF•6H_2O also produced diffraction grade crystals of another related system, namely **1**$^{4+}$•**4**$_2$•9.5H_2O. In the single crystal of [**1**$^{4+}$•**4**$_2$•9.5H_2O] the pseudorotaxane core, [**1**$^{4+}$•**4**]$^{2+}$, is structurally similar to that observed in the single crystal of [**1**$^{4+}$•**4**$_2$•DMF•5.5H_2O] and [**1**$^{4+}$•**4**$_2$•DMF•6H_2O]. As highlighted by Figure S49, in the case of [**1**$^{4+}$•**4**$_2$•9.5H_2O], a 1D self-assembled complex is seen that built up from individual pseudorotaxane units, as well as a bridging molecule of **4**. Based on the structural features, the extended arrangement is stabilized by π-π donor-acceptor interactions.

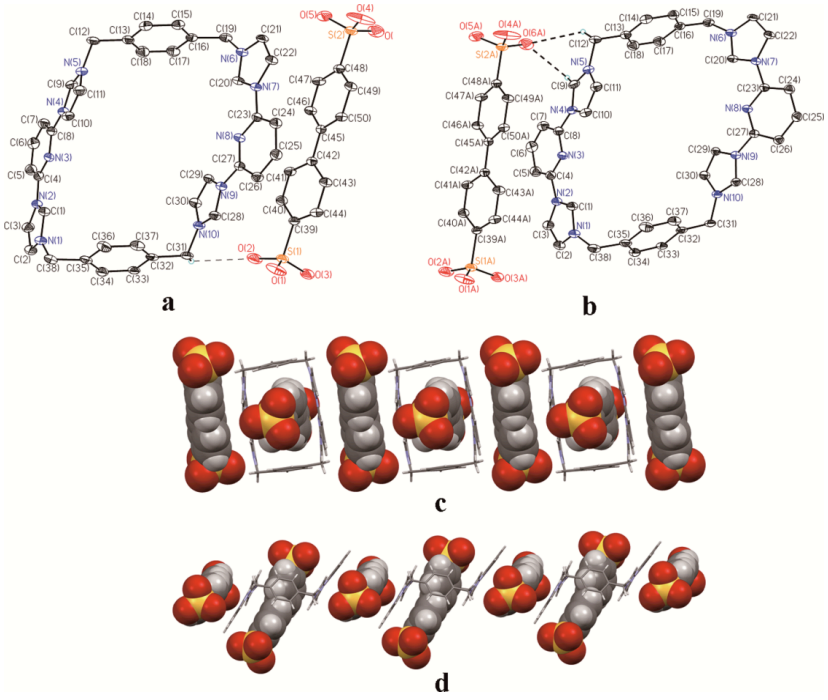

Figure S49. Partial single crystal packing diagram showing the 1D 'DAD' self-assembled structure present in complex $\mathbf{1}^{4+}\bullet\mathbf{4}_2\bullet 9.5H_2O$. The views presented here are designed to highlight the interaction between two neighboring pseudorotaxane "monomer" units present in the extended structure. Views (a) and (b) show the atom labeling scheme of the complex with only the molecule of **4** bound the outer periphery being shown (the threaded molecule of **4** has been removed for clarity), while views (c) and (d) show side perspectives of the 1D 'DAD' self-assembled complex. Inter-complex π···π interactions were inferred from the following selected interatomic distances [Å]: N(10)...O(2) 3.220(9), C(21)...O(5) 350(1), C(28)...O(1) 3.61(1), C(28)...O(2) 3.493(9), C(40)...N(9) 3.46(1), C(40)...C(27) 3.74(1), C(40)...C(29) 3.62(1), C(41)...N(8) 3.596(9), C(41)...N(9) 3.73(1), C(41)...C(27) 3.57(1), C(42)...N(8) 3.686(9), C(42)...C(23) 3.75(1), C(42)...C(27) 3.70(1), C(43)...C(25) 3.69(1), C(43)...C(26) 3.61(1), C(44)...C(26) 3.67(1), C(45)...N(7) 3.760(9), C(45)...C(23) 3.52(1), C(45)...C(24) 3.73(1), C(46)...N(7) 3.632(9), C(47)...N(7) 3.79(1), C(47)...C(22) 3.73(1), C(48)...C(22) 3.59(1), N(5)...O(6A) 3.47(1), C(2)...O(3A) 3.42(1), C(3)...O(3A) 3.62(1), C(42A)...C(4) 3.61(1), C(42A)...C(5) 3.68(1), C(43A)...N(2) 3.46(1), C(43A)...C(1) 3.71(1), C(43A)...C(4) 3.58(1), C(44A)...N(2) 3.62(1), C(44A)...C(2) 3.78(1), C(44A)...C(3) 3.58(1), C(45A)...C(7) 3.77(1), C(43A)...C(8) 3.75(1), C(46A)...C(6) 3.65(1), C(46A)...C(7) 3.61(1), C(47A)...C(7) 3.72(1), C(49A)...N(4) 3.54(1), C(49A)...C(8) 3.78(1), C(49A)...C(10) 3.79(1).

References:

1 W. L. F. Armarego, C. L. L. Chai. *Purification of Laboratory Chemicals (fifth edition)*, Elsevier Science: USA (2003).

2 H. E. Gottlieb, V. Kotlyar, A. Nudelman. *J. Org. Chem.*, **1997**, *62*, 7512-7515.

3 J. N. Abelson, M. I. Simon, C. W. Carter Jr, R. M. Sweet. Methods in Enzymology, 276: Macromolecular Crystallography, Part A, 307 - 326, Academic Press (1997).

4 A. Altomare, M. C. Burla, M. Camalli, G. L. Cascarano, C. Giacovazzo, A. Guagliardi, A. G. G. Moliterni, G. Polidori, and R. Spagna. *J. Appl. Cryst.*, **1999**, *32*, 115-119.

5 G. M. Sheldrick. SHELXL97. Program for the Refinement of Crystal Structures. University of Gottingen, Germany, 1994.

6 $R_w(F^2) = \{w(|F_o|^2 - |F_c|^2)^2/w(|F_o|)^4\}^{1/2}$, where w is the weight given each reflection. $R(F) = (|F_o| - |F_c|)/|F_o|\}$ for reflections with $F_o > 4((F_o))$. $S = [w(|F_o|^2 - |F_c|^2)^2/(n - p)]^{1/2}$, where n is the number of reflections and p is the number of refined parameters.

7 A. J. C. Wilson, International Tables for X-ray Crystallography. Vol. C, Tables 4.2.6.8 and 6.1.1.4. Boston: Kluwer Academic Press (1992).

8 G. M. Sheldrick. (1994). SHELXTL/PC (Version 5.03). Siemens Analytical X-ray Instruments, Inc., Madison, Wisconsin, USA.

9 P. Job, *Ann. Chim. (Paris)*, **1928**, *9*, 113-203.

10 Hyperquad2003: P. Gans, A.Sabatini, A. Vacca, *Talanta*, **1996**, *43*, 1739-1753.

11 M. Ōki, Applications of Dynamic NMR Spectroscopy to Organic Chemistry; VCH, Weinheim, 1985.

12 D. Neuhaus, M. P. Williamson, *The Nuclear Overhauser Effect in Structural and Conformational Analysis*; VCH Publishers; Cambridge, U. K., 1989.

13 H. Friebolin, Basic One- and Two-Dimensional NMR Spectroscopy; WILEY-VCH, Weinheim, 2005.